Analysis of Low Cost Permanent Magnet and Reluctance Electrical Machines with Different Rotor Anisotropy for Variable Speed Drive

by

Md Jabed Hossain

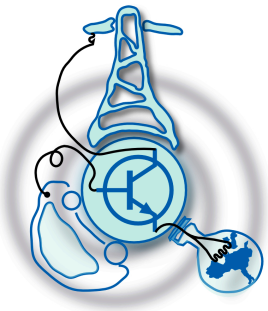

Submitted to the Department of Electrical Engineering, Electronics, Computers and Systems
in partial fulfillment of the requirements for the degree of

Erasmus Mundus Master Course in Sustainable Transportation and Electrical Power Systems

at the

UNIVERSIDAD DE OVIEDO

September 2017

Author .....

Certified by .....

Michele Degano
Assistant Professor
Thesis Supervisor

Analysis of Low Cost Permanent Magnet and Reluctance Electrical Machines with Different Rotor Anisotropy for Variable Speed Drive

by

Md Jabed Hossain

Submitted to the Department of Electrical Engineering, Electronics, Computers and Systems
on September 09, 2017, in partial fulfillment of the
requirements for the degree of
Erasmus Mundus Master Course in Sustainable Transportation and Electrical Power Systems

Abstract

This thesis deals with the electromagnetic design of low cost Permanent Magnet Synchronous Motor (PMSM) with different rotor anisotropies as well as two types of Synchronous Reluctance (SynR) machines. Six machines have been compared and analysed on the basis of same stator winding and the number of poles. This thesis conducts holistic approach to investigate maximum torque per ampere (MTPA) angle for each topology.

The main objective of this work is to investigate some of the key machine performance, in order to investigate the electromechanical characteristics such as, power, efficiency, torque, PM flux linkage, d-q axes synchronous inductances, saliency ratio and current characteristics with all operating speed range and in various loading conditions. This analysis is conducted by means of finite element analysis (FEM) and mathematical formulations.

This thesis presents an analytical model for surface mount permanent magnet (SMPM) and results are verified with FEM. In addition, SMPM, Inset permanent magnet (PMs) and Interior PMs machines are optimized by reducing the air gap in order examine performance with their base model.

Moreover, an analytical model to estimate the iron loss in PMs machine is developed and included in the designed procedures. However, flux density values in areas corresponding to stator teeth and back iron core were taken from results of FEMM for using in the iron loss model.

Finally, this thesis presents the effects of magnet on d-q inductances in PMs machines configuration are studied and their results are compared to each others.

Thesis Supervisor: Michele Degano
Title: Assistant Professor

Acknowledgments

I would like to thank my honourable and esteemed supervisor Professor Michele Degano. I am sincerely thankful to him for his prompt support concerning any problems I have encountered during the whole work.

A special thank goes to Dr. Mahmoud Hanafy for helping me to solve various difficulties are greatly appreciated. I am very grateful to EMMC STEPS coordinator, Professor Pablo Garcia Fernandez and STEPS committee members for their continued and exemplary guidance in the entire journey with Erasmus Mundus Master Course in Sustainable Transportation and Electrical Power Systems (EMMC STEPS).

At last, I would like to extend my gratitude to my parents, my elder brother and especially my lovely wife for their understanding and moral support during my studies.

Contents

List of Figures

List of Tables

Chapter 1

Introduction

This chapter provides background information of the thesis; it also illustrates the objective and scope of the thesis. This chapter closes with a summery of the thesis deliverables.

1.1 Objective of Thesis

The consumptions of electrical energy especially for electric motor loads is rising rapidly over the last few decades which is accounted for 35%–40% of the generated electrical energy worldwide and which is expected to increase in the coming years [5]. So, there is crucial need for designing energy efficient machine. Nowadays, it has been proven that high efficient machine can lead to reduction of energy consumptions. For example, Permanent Magnet Synchronous Motor (PMSM) is superior because it normally uses high strength rare earth permanent magnets (PMs) and consequently provides high torque density, high efficiency and robust rotor structure for the application of electric propulsion systems. It has been paid more and more attention because of its wide range of degree of freedom in designing.

This thesis aims to carry out comparative investigations of low cost PMs machine (in particular ferrite PMs) with different rotor anisotropies and other machine topologies with reluctance properties. This analysis will be carried out using analytical and finite element analysis tools, consider stator distributed winding configuration. Investigation will be carried out in order to evaluate some key electromechanical parameters

such as MTPA angle for each machine, torque pulsation, the iron loss and copper loss, d- and q-axis flux linkage and d- and q-axis inductances.

1.2 Background and Scope of Project

In the first phase of thesis, focus is given to design and compare four specific machines as shown from Figure 3-1 to Figure 3-4 such as Surface Mount Permanent Magnet (SMPM), Inset Permanent Magnet Machine (IPM) Machine, Interior Magnet (or buried) Permanent Machine and Permanent Magnet Assisted Synchronous Reluctance (PMASR) machine. This study has been conducted keeping constant the following parameters:

- Stator geometry
- Stack length
- Air gap length
- Current loading

Ferrite magnetic material is used for each machine topologies as it has some advantages with respect to Neodymium Iron Boron (NdFeB) rare earth magnets, as summarised below:

- Ferrite is low cost permanent magnet.
- Price of Ferrite keeps stable throughout the year.
- Price of rare earth PMs such as NdFeB and SmCo is increasing day by day.
- Ferrite has a positive reversible temperature coefficient of coercivity which yields to better motor performance.
- Rare earth magnets are subjected to environmental effects and are responsible for greenhouse gas emission at extraction and processing time, on the other hand, Ferrite is exempted from this blame.

By considering above mentioned merits, focus is given to use low cost ferrite material in studied topologies explained in earlier.

Moreover, PM machines with rare earth PMs such as NdFeB could also be subjected to demagnetisation with exposed to high temperature. Therefore, in some particular applications where reliability is a major concern over a wider operating loading, this thesis is planned to carried out to single out which topologies is the most reliable with respect to others for particular application.

So, the choice among different topologies depends on a careful calculation of the electromechanical performance requirements for particular applications to select the best option for meeting the requirements.

For this reason, in the second part of this thesis, the same analysis is carried out for Synchronous Reluctance (SynR) machine as shown in Figure 3-5. In addition, a new topology is called Segmented REL (SEG REL), as shown Figure 3-6, SEG REL follows the same operating principle of SynR machine is also analysed in this thesis.

In salient pole PMSM, for given rated current torque varies as a function of advance angle,γ, for which it gives the maximum efficiency. There is a co-relation between rated current and advance angle: the higher the rated current correspond to greater the advance angle. Therefore, for given rated current there is a unique value of γ which will maximize the torque. First of all, value of γ needs to be determined for rated current in every topologies and then other measurements are carried out.

The purposes of this thesis are summarized as follows:

- to create suitable simulation model in order to calculate the Maximum Torque Per Ampere Current (MTPA) angle for all topologies.
- to determine the inductance profile for different current loading.
- to create a magnetic modelling in d-q reference frame in order to control the speed and torque at different working conditions.
- to develop skills pertaining to analysis of modern electrical machines for variable speed drive.

- to acquire ability to calculate the losses at different stage of the machine.
- to create an Iron loss model in FEM environment.
- to develop an analytical calculation model of SMPM machine and its results are compared with FEM results.
- to learn how to make appropriate documentation of comparative study among machines with different rotor anisotropy.

1.3 Organization of Thesis

PMs motor's operation and state of art researches pertaining to rotor anisotropy are presented in chapter 2. Chapter 3 discusses the approaches to design FEM models of six topologies. Analytical analysis of SMPM machine along with comparison of FEMM model of same machine is illustrated in chapter 4. Chapter 5 describes FEMM results of first four models considered under this study. Similarly, results of FEMM for synchronous reluctance motor and segmented reluctance motor are explained in Chapter 6. Finally, conclusions have been drawn and expected works still to be completed are described in chapter 7.

Chapter 2

PMs Motors Operation and Literature Review

PMSM has higher degree of freedom in making rotor structure and machine can be designed for large number of poles and diameters. PMSM are advantageous in many ways.

There are no losses in rotor since no magnetising current requires for the rotor field. Also, it is kind of machine with the highest torque/ power density in all the machine types. In addition, very simple rotor structure with low inertia facilitates the low manufacturing cost. Finally, flux lines can be directed by making different rotor structure, for example, axial flux and transverse flux machine.

However, price of rare earth magnets are increasing day by day which pushes higher price of PMSM. Moreover, it is not suitable working at higher temperature condition sometimes losses magnetism at higher temperature. Main drawback is that it cannot be operated from mains which requires power converter.

2.1 Working Principles of PMSM

Magnetic field of PMSM is created from PMs which is affixed on the rotor in order to create rotor magnetic field. Three phase set of voltage is applied to the stator windings which produces three phase current flow in the stator windings. These three phase set of currents create a magnetic field which is revolving at synchronous

speed. Rotor magnetic field tries to lock with stator magnetic field according to the principles of magnets. Since the stator magnetic field is rotating, rotor magnetic field also rotating at synchronous speed, once both the magnetic fields lock each others.

The fixed magnetic field in the rotor of PMs motor cannot use to induction process in order to start the motor. However, PMs motor requires a drive system at the starting. The drive is nothing but a real inverter, an electronic controller where algorithms are implemented. Algorithms are updated at a rate of $10,000$ times per second with aid of digital devices which makes PMs motor sophisticated where precision is real issues. It is possible to generate required magnitude of voltage and frequency by controlling gate pulse of inverter with pulse width modulation (PWM) techniques. Torque of the PMSM is the product of current amplitude and the phase relation between currents and magnetic axis. So, the continuous knowledge of rotor angle is necessary in order to control the PMs motors.

2.2 Three Phase Model of PMSM

Kirchhoff's voltage law equation for a PMSM is expressed as

$$V_\phi = E_A + jX_S I_A + I_A R_A \tag{2.1}$$

here,

V_ϕ = Applied phase voltage

E_A = Back e.m.f in phase A

X_S = Synchronous reactance

I_A = Current in phase A

R_A = Resistance in phase A

Stator equivalent circuit of PMSM is shown in Figure 2-1 and corresponding phasor diagram is shown in Figure 2-2. Phasor is drawn by considering motor as leading load. Resistive drops has been ignored in this phasor since it is negligible with respect synchronous reactance drops. It is shown from the phasor diagram that average power

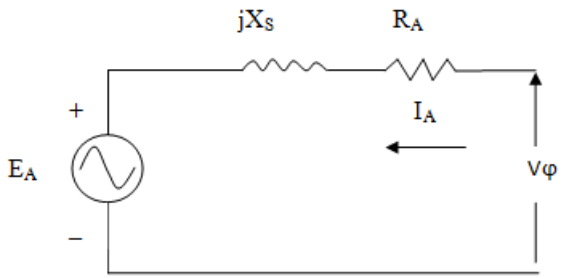

Figure 2-1: Stator equivalent circuit of PMSM for single phase

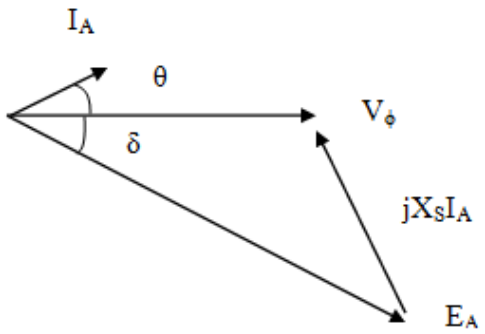

Figure 2-2: Phasor diagram of PMSM for single phase

produce by three phase machine is expressed by the following equation

$$P = \frac{3}{2} V_\phi I_A \cos\theta \tag{2.2}$$

It is assumed that machine is lossless, so,terminal voltage,V_ϕ, is equal to internal generated voltage, E_A, consequently above equation becomes

$$P = \frac{3}{2} E_A I_A \cos(\theta - \delta) \tag{2.3}$$

Power is the product of the torque and the mechanical rotational speed ,$\frac{\omega}{p}$, which is expressed as

$$P = \frac{\omega}{p} T \tag{2.4}$$

where small letter p is the value of pole pairs.

Torque is determined in terms of terminal quantities as follows

$$T = p\frac{3}{2}\lambda_A I_A \cos(\theta - \delta) \tag{2.5}$$

where λ_A is the flux linkage of phase A.

Phase inductance is measured as a function of rotor position since flux path in the rotor always changes with the electrical rotor position θ. So, self inductances are evaluated with regard to electrical rotor position as follows.

$$L_A(\theta) = L_{ls} + L_{0s} - L_{2s}\cos(2\theta) \tag{2.6}$$

$$L_B(\theta) = L_{ls} + L_{0s} - L_{2s}\cos(2\theta + \frac{2\pi}{3}) \tag{2.7}$$

$$L_C(\theta) = L_{ls} + L_{0s} - L_{2s}\cos(2\theta - \frac{2\pi}{3}) \tag{2.8}$$

Mutual inductance between two phases can be written as

$$M_{AB}(\theta) = -\frac{1}{2}L_{0s} - L_{2s}\cos(2\theta - \frac{2\pi}{3}) \tag{2.9}$$

$$M_{AB}(\theta) = -\frac{1}{2}L_{0s} - L_{2s}\cos(2\theta + \frac{2\pi}{3}) \tag{2.10}$$

$$M_{AC}(\theta) = -\frac{1}{2}L_{0s} - L_{2s}\cos(2\theta) \tag{2.11}$$

Flux produce by permanent magnet can also be expressed by function of rotor position as follows

$$\phi_A(\theta) = \Phi_M \cos(\theta) \tag{2.12}$$

$$\phi_B(\theta) = \Phi_M \cos(\theta - \frac{2\pi}{3}) \tag{2.13}$$

$$\phi_C(\theta) = \Phi_M \cos(\theta + \frac{2\pi}{3}) \tag{2.14}$$

2.3 d-q Reference Model of PMSM

Three phase PMSM model can be transformed into d-q reference frame model by applying the park transformation. In d-q reference frame direct axis or d-axis is aligned with the direction of the magnet flux,Ψ_m, or Ψ_f as shown in Figure 2-3 whereas q-axis bisects the section between permanent magnets. Since the magnet is embedded in the rotor, magnet flux rotates with speed of rotor as well as speed of the magnetic flux created in the stator.

I_q currents in the d-q reference frame creates mmf in the q direction is called torque current. Similarly, I_d currents create mmf in the d direction is called the field current. Positive I_d current helps magnet flux to create more magnetic flux but not so much because Iron will be near saturation point. Negative I_d currents decrease the magnet flux in other words weakens the magnetic field. Saliency occurs in the PMs

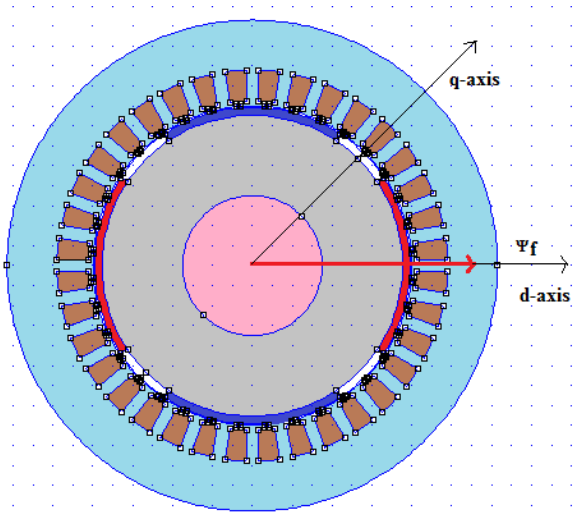

Figure 2-3: Magnet flux is aligned with d-axis in SMPM machine

machine when stator current see the preferred magnetic direction.

Three stationary coils which are placed 120 degree apart can be represented as two stationary α and β reference frame. Voltage equations of PMSM in two stationary α and β reference frame are as follows

$$v_{s\alpha} = i_{s\alpha} R_s + \frac{d}{dt}\Psi_{s\alpha} \tag{2.15}$$

$$v_{s\beta} = i_{s\beta} R_s + \frac{d}{dt}\Psi_{s\beta} \tag{2.16}$$

where,

R_s = Resistance expressed in the stationary coil in the stator

$\Psi_{s\alpha}$ = Magnetic flux in the α axis

$\Psi_{s\beta}$ = Magnetic flux in the β axis

$i_{s\alpha}$ = Current measured in α axis

$i_{s\beta}$ = Current measured in β axis

Magnetic flux of each axis is consisting of two parts flux due to magnet flux and stator current. Magnetic fluxes can be expressed as follows

$$\Psi_{s\alpha} = \Psi_m \cos\theta_r + L_s i_{s\alpha} \tag{2.17}$$

$$\Psi_{s\beta} = \Psi_m \sin\theta_r + L_s i_{s\beta} \tag{2.18}$$

where,

L_s = Inductance of both axis

Ψ_m = Magnet flux

From equations (2-17) and (2-18), we may rewrite equations (2-15) and (2-16) as

$$v_{s\alpha} = i_{s\alpha} R_s + \frac{d}{dt}(\Psi_m \cos\theta_r + L_s i_{s\alpha}) \tag{2.19}$$

$$v_{s\beta} = i_{s\beta} R_s + \frac{d}{dt}(\Psi_m \sin\theta_r + L_s i_{s\beta}) \tag{2.20}$$

After transforming into park transformer voltage equations (2-19) and (2-20) yield,

$$v_d = R_s i_d + L_d \frac{di_d}{dt} - \omega_r L_q i_q \tag{2.21}$$

$$v_q = R_s i_q + L_q \frac{di_q}{dt} + \omega_r L_q i_d + \omega_r \Psi_m \tag{2.22}$$

where,

L_d = d-axis inductance

L_q = q-axis inductance

i_d = d-axis current

i_q = q-axis current

ω_r = rotating speed of d-q reference frame

d-axis flux linkage is given by

$$\Psi_d = L_d i_d + \Psi_m \tag{2.23}$$

And q-axis flux linkage is given by

$$\Psi_q = L_q i_q \tag{2.24}$$

d-axis voltage equation can be written as in circuit form

$$v_d = R_s i_d + \frac{d\Psi_d}{dt} - \omega_r \Psi_q \tag{2.25}$$

$$v_d = R_s i_d + \frac{d}{dt}(L_d i_d + \Psi_m) - \omega_r \Psi_q \tag{2.26}$$

It is assumed that magnet flux consists of L_{md} and i_m

$$\Psi_m = L_{md} i_m \tag{2.27}$$

Putting the value of Ψ_m in previous equation(2.26) yields

$$v_d = R_s i_d + \frac{d}{dt}[i_d(L_{md} + L_{ld}) + L_{md} i_m] - \omega_r \Psi_q \tag{2.28}$$

$$v_d = R_s i_d + \frac{d}{dt}[L_{md}(i_m + i_d) + L_{ld} i_d] - \omega_r \Psi_q \tag{2.29}$$

where,

L_{md} = d-axis magnetizing inductance

L_{ld} = d-axis leakage inductance

$\omega_e \Psi_q$ = armature reaction drops

Equivalent circuit of d-axis PMSM has been drawn, as shown in Figure 2-4, on the

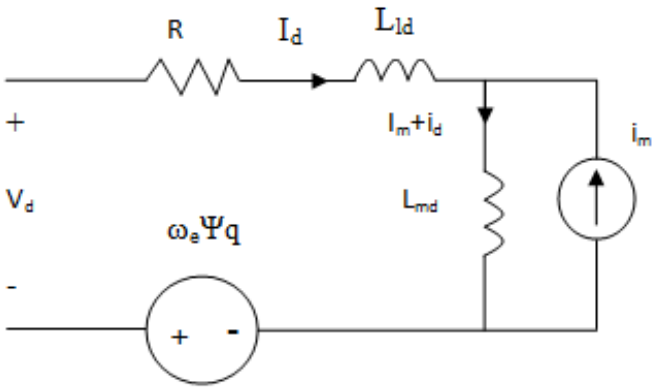

Figure 2-4: d-axis equivalent circuit of PMSM

basis of the equation(2.29). I_m current is considered empirically as magnetization current of permanent magnet. Permanent magnet flux is distorted by the q-axis flux and this effect is called armature reaction in PMSM and its drops $\omega_e\Psi_q$ is included in equivalent circuit.

q-axis voltage equation can be written as in the circuit form

$$v_q = R_s i_q + L_q \frac{di_q}{dt} + \omega_r (L_d i_d + \Psi_m) \tag{2.30}$$

$$v_q = R_s i_q + (L_{mq} + L_{lq}) \frac{di_q}{dt} + \omega_r \Psi_d \tag{2.31}$$

where,

L_{mq} = q-axis magnetizing inductance

L_{lq} = q- axis leakage inductance

$\omega_r\Psi_d$ = back emf voltage

q-axis equivalent circuit of PMSM is drawn in Figure 2-5 based on equation(2.31). Back emf voltage is adding with applied v_q stator voltage. Torque production in PMSM in d-q reference frame is given by the following equation:

$$Torque, T = k\left(\Psi_d i_q - \Psi_q i_d\right) \tag{2.32}$$

where,

k = constant

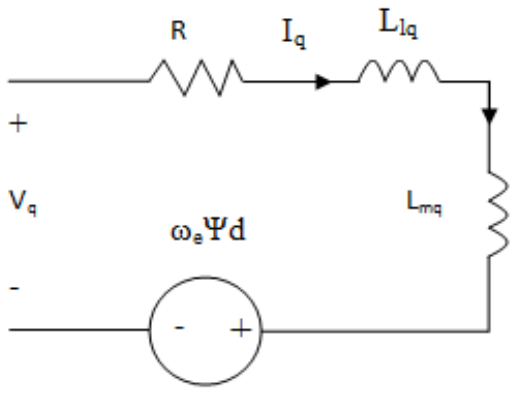

Figure 2-5: q-axis equivalent circuit of PMSM

for rms convention, $k = \frac{3p}{2}$

p = Pole pairs

By substituting equations (2.24) and (2.25) into equation (2.32), we obtain

$$T = k\left[\Psi_m i_q + i_d i_q \left(L_d - L_q\right)\right] \tag{2.33}$$

Equation representing torque is produced by PMSM can be split into two parts. First term of this equation is called magnet alignment torque because it originates from permanent magnet flux.

$$T_{magnetic} = \frac{3p}{2}\Psi_m i_q \tag{2.34}$$

The other component is coming from rotor saliency effect is called reluctance torque

$$T_{reluctance} = \frac{3p}{2} i_d i_q (L_d - L_q) \tag{2.35}$$

It is seen from equation (2.33), torque production in PMSM depends on variables of Ψ_m, i_d, i_q, L_d and L_q. It is possible to calculate infinite number of combinations of i_d and i_q currents to produce same amount of torque without thinking of inductances combinations. Magnet alignment torque is directly proportional to the magnitude of i_q currents with Ψ_m keeping constant. Since the flux path of d and q axis of SMPM machine are equal, magnitude of L_d is equal to L_q as a result reluctance torque becomes zero. Resultant torque of SMPM machine is only equal to magnet

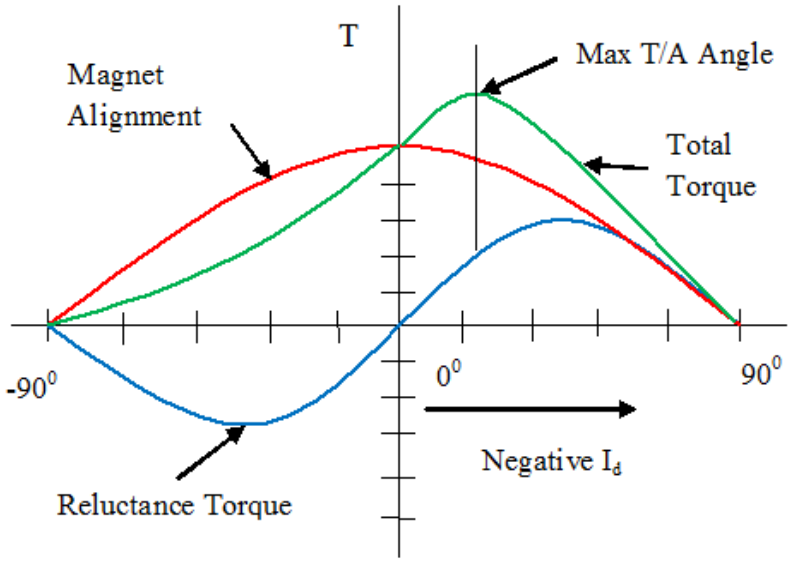

Figure 2-6: Representation of different torques in PMs machine

alignment torque which denotes red curve in Figure 2-6.

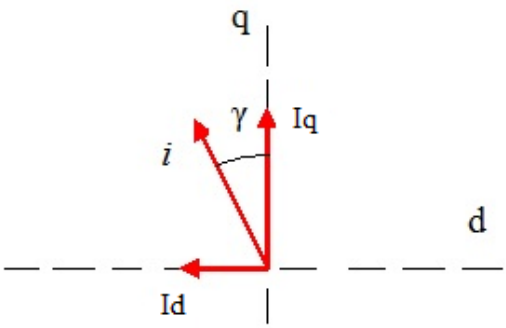

Figure 2-7: Advance angle representation

Permanent magnet has lower permeability or higher reluctance than iron, so the value of Inset and Interior PMs machine direct axis inductance, L_d, lower than that of quadrature axis inductance, L_q. This resulting saliency includes reluctance torque in torque calculation in salient pole machine. Positive i_d current yields negative reluctance torque which reduces the magnetic alignment torque. But negative i_d current produces positive reluctance torque which increases total torque. So, there exists a particular pairs of i_d and i_q currents for which torque is maximum for specific phase current. It is always desirable to operate machine as close as the desired current pairs.

Angle of phase current determines the magnitude of i_d and i_q currents. So,determining current angle for which torque is maximum plays a vital role in controlling of PMSM in other words this controlling is called MTPA control.

Maximum torque point can be determined by differentiating the torque equation (2.33) and set equal to zero, so maximum torque point , γ_{maxT}, we obtain

$$\gamma_{maxT} = sin^{-1}\left\{\frac{-\Psi_m \pm \sqrt{\Psi_m^2 + 8\left|i\right|^2}\Delta L^2}{-4\Delta L\left|i\right|}\right\} \tag{2.36}$$

The angle between q-axis and phase current vector is called advance angle as shown in Figure 2-7. Advance angle determines the maximum torque for specific current in salient pole machine.

2.4 Losses of PMSM

This section explores different losses of PMSM and explains general equation to calculate these losses. Main losses of PMSM are copper loss, Iron loss (hysteresis loss and eddy current loss), windage loss and stray loss. Copper and Iron losses are two primary types of losses occurring in electrical machine. Windage (also referred to as mechanical loss) and stray losses are often ignored in the total loss calculation.

2.4.1 Copper Losses

Copper loss is due to heat produced by electrical current in the conductor. When electrical current flows in the conductor some energy are dissipated due to resistance of the windings. Copper loss constitutes the maximum losses in the machine. The equation for Copper loss calculation can be expressed

$$P_j = 3RI_n^2 \tag{2.37}$$

here,

R = Winding resistance per phase

I_n = RMS value of phase current

Windings resistance per phase can be determined by following equation (2.38)

$$R = \rho_{cu} \frac{N_{ph}(L_{stk} + L_{ew})}{S_{cu}} \tag{2.38}$$

where,

ρ_{cu} = Copper resistivity

L_{stk} = Stack length

L_{ew} = Lengths of copper conductor

S_{cu} = Cross-section of copper conductor

2.4.2 Iron Loss

The accurate calculation of iron loss is very strenuous task in order to design a machine precisely. There are several methods to calculate the iron loss component, such as, frequency domain model and time domain model. In this analytical analysis, frequency domain model have been used to determine the iron losses in the stator. This model is used separately to evaluate iron losses in the back iron and the tooth since the flux density is varied between tooth and back iron region in the stator. Summation of both losses is the total iron loss of the machine since iron loss of the rotor is not considered.

$$P_{spec} = P_{spec\_fe} \times (\frac{B_{max}}{B_{fe\_ref}})^2 \times [k_{hy} \times \frac{f_{elect}}{f_{ref}} + k_{ed} \times (\frac{f_{elect}}{f_{fe\_ref}})^2] \tag{2.39}$$

where,

P_{spec_fe} = Iron losses coefficient

B_{max} = Maximum flux in the considered region

B_{fe_ref} = Reference iron flux density for iron losses calculation

f_{elect} = Electrical frequency for the base speed

f_{fe_ref} = Reference frequency for iron loss calculation

k_{hy} = Specific coefficient of hysteresis loss

k_{ed} = Specific coefficient of eddy current loss

This iron loss calculation model includes two components hysteresis loss and eddy current loss. The spasmodic movement within block walls creates eddy currents. In addition, it can be induced in nearby standstill coil by influence of changing magnetic field. Eddy current creates a magnetic field which opposes the main magnetic field. Hysteresis loss is happened due to magnetic domain requires some power in order to change the orientation. So, hysteresis loss depends on frequency and magnetic flux density.

2.4.3 Windage Loss

Windage losses refer to the losses caused by the friction between air and rotor surface. It depends on shape of the rotor, for example, salient pole machine suffers more windage losses than non-salient machine.

2.4.4 Stray Loss

Stray losses are very difficult to calculate. All of the following factors may cause the Stray losses:

- current flow through the core
- harmonic in the core
- distortion of magnetic flux due to armature reaction
- short circuit currents in the coil.

2.5 Importance of Rotor Anisotropy on Field Weakening Operation

Field weakening operation can be explained based on working principle of Synchronous motor operation where field flux is controlled by varying the dc current. Some definitions need to be clarified before explaining field weakening operation. Torque is proportional to the product of armature current and the magnetic flux in the d-axis. Induced voltage in the armature circuit is the proportional to the product of mechanical speed of rotor and magnetic flux. Voltage and power increase with

the increasing mechanical speed of rotor but torque remains constant with the rated current and rated flux as shown in Figure 2.8, this region is called constant torque region. The speed when machine gains the rated voltage is called base speed or rated speed. The speed above the base speed power is fixed since voltage is fixed; this region is called constant power. In order to increase the speed above the base speed flux must be decreased as voltage is product of flux and speed. Power is the product of torque and mechanical speed. Torque must be decreased as power is constant above the base speed.

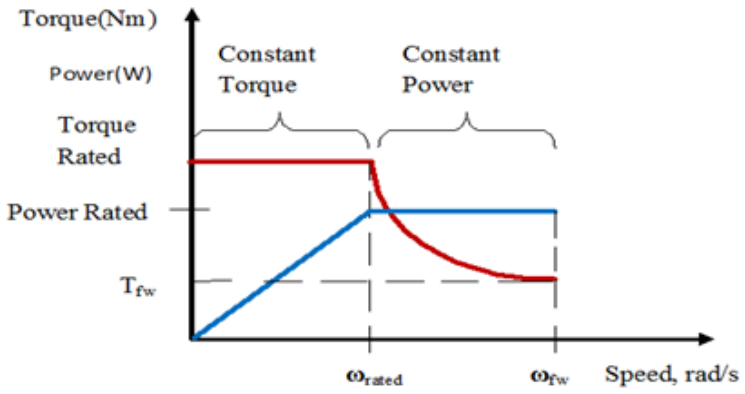

Figure 2-8: Field weakening principle

In PMs motors flux is achieved by permanent magnet in the rotor. So, field flux can only be controlled by introducing i_d currents which is originated from the armature current. At rated speed, machine gains the rated voltage, which is called voltage limit contour is expressed as by the following equation

$$v_b^2 \geq \omega^2[(\Psi_m + L_d i_d)^2 + (L_d i_d)^2] \tag{2.40}$$

In order to increase speed above the rated speed, negative i_d current needs to be imposed to bring back voltage vector to a voltage limit as shown in Figure 2-9.

In case of steady state, ω_r is considered eaqual to ω_e then, d- and q-axis voltage equations become as follows

$$v_d = Ri_d - \omega_e L_q i_q \tag{2.41}$$

$$v_q = Ri_q + \omega_e L_d i_d + \omega_e \Psi_m \tag{2.42}$$

$$E = \omega_e \Psi_m \tag{2.43}$$

So, the phasor equations are

$$v_d = Ri_d - \omega_e L_q i_q \tag{2.44}$$

$$v_q = Ri_q + \omega_e L_d i_d + E \tag{2.45}$$

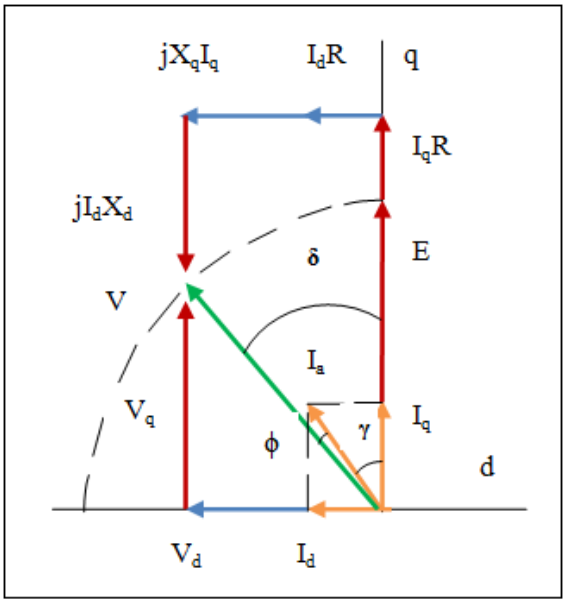

Figure 2-9: Phasor diagram of PM machine with negative i_d currents

If a motor runs above the base speed total voltage exceeds the voltage limit, so negative i_d current helps total voltages to bring back into voltage limit as shown in Figure 2-9. Anisotropy plays an important role in field weakening operation. Several studies have been conducted by researchers and demonstrate that speed range can be extended in the constant power region by choosing the suitable motor parameters. They suggest that maximum torque per ampere can be achieved by adjusting optimal alignment of the magnetic field and stator slots .

2.6 Literature Review

Over the last few years, developing energy efficient, wide speed range, constant torque and low torque ripple electrical machine concept has been pivotal research topic among scientists as it has enormous potential to achieve a reliable and efficient operation for variable speed drives. Sheer volume of researches, in the field of PMs electrical machine, is dedicated to investigate their electromechanical performance.

For example, it was shown that peak torque of SMPM machine 35 percent higher than Reluctance (REL) [4] machine though REL machine is the lowest cost machine. SMPM machine shows better performance around the base speed with respect to other topologies almost in every electromagnetic performance, but it is not always suitable for the wide speed range of application because of worst performance in Field Weakening (FW) region.

In order to get the same amount of torque in Permanent Magnet Assisted Synchronous Reluctance (PMASR) machine, current needs to increase 10 percent more than current required in SMPM. However, in Synchronous Reluctance machine saturation of magnetic flux is much lower than SMPM machine because of absence of magnet in the rotor structure.

Scientists have shown that Synchronous reluctance motors having segmented rotor structure helps a lot to reduce the torque ripple due to the rotor anisotropy [6]. Synchronous reluctance machine having high anisotropy is good for high performance application such as in robotics where low torque ripple is an important implications.

Interior PMs machine has gained increasing attention in recent years in the high speed applications [7]. They have higher torque density than SMPM because they have two different torques such as reluctance torque due to rotor saliency and the magnetic torque due to the permanent magnets. They also have more degree of freedom in the FW region than SMPM.

SMPM machine is not an ideal candidate beyond the base speed but inclusion of fractional slot concentrated windings (FSCW) into SMPM machine makes it possible to boost slot copper fill factor and the phase inductance which are the requirements

to withstand the field weakening [9] region.

Saturation of the magnetic field can be done by inducing high stator current in the stator thus introduces saliency into a normally symmetric machine [10]. This momentarily saliency helps to increase torque up to 4% extra output torque than the torque is produced for the same maximum stator current.

The Inset or Buried Magnet configuration is advantaged by its large magnetic path in the rotor. As a result, rotor iron saturation is very low and rotor saliency can be detected even at the over loading conditions [1]. This property allows detection of the correct rotor angle of an inset PM motor by using a sensor less control technique.

Interior permanent magnet takes advantage of both magnetic torque and reluctance torque but the main drawback is the high torque ripple. The induced back-EMF in this machine is not pure sinusoidal which causes significant torque ripple when it is feed by ideal sinusoidal current source. Researcher have worked on it and optimum current waveforms are proposed and demonstrated to compensate the harmonic components in the back-emf and reduce torque ripple as well [8].

Small airgap and highly anisotropy in the rotor structure is always considered to reduce torque ripple in SynREL and IPM machine [2]. In addition with these, an optimization is required to evaluate the optimal rotor geometry so as to get smooth torque. Researchers have shown that torque ripple have been affected with the small variation in stator and rotor geometry.

Boroujeni, et all, [3] have develop an analytical model in order to predicting the airgap flux density and armature reaction in the slotless surface-inset PM machines. The concept of magnetisation surface current (MSC) is used in modelling process. Instead of using rotor poles in the modelling process some MSCs are considered on the boundaries of the removed rotor poles.

In recapitulate, recent researches on low cost PMs machine with different rotor anisotropy is not fulfilled because most of the researchers analysed some of the machine's key electromechanical performances, moreover, comparison was done between two or mostly among three rotor topologies. So, further research is needed to reduce this gap. This thesis will investigate complete electromechanical performance char-

acteristics and compare the advantages of one topology over others for six different rotor topologies.

Chapter 3

Design Procedures

This chapter concentrates on design procedures of different machines in FEMM environment. There are some aspects such as thermal, saturation, insulation and rated performance which are not considered in FEM analysis. In the first section of the chapter design specification will be given. This chapter ends giving a brief explanation about the analysis procedures of these machines.

3.1 Design Specification

This section discloses the design specification of six different machines from Table 3.1 to Table 3.4. Table 3.1 reveals the general design specification of motor.

Table 3.1: General Design Specification for Motor

Symbol	Parameters	Value
p	Number of pole pairs	2
L_{stk}	Stack length	220mm
n_c	Number of conductor in one slot	1
k_{fill}	Slot fill factor	0.4
S_{slot}	Slot area	$155.12mm^2$
B_{rem}	Remnant magnetic flux density	0.35T
μ_r	Relative permeability of magnet	1
σ_{cu}	Copper conductivity at 20°C	59×10^7 S/m
k_w	Winding coefficient	1

Table 3.2 gives the stator design parameters that are applicable for all machines since the stator structure of all machines under study are identical. In the following

Table 3.2: Design Specification for Stator

Symbol	Parameters	Value
D_e	External diameter	246mm
D_s	Inner diameter at the air gap	160mm
Q_s	Slot number	36
h_s	Slot height	18mm
w_t	Tooth width	6.2mm
w_{so}	Slot opening width	2mm
h_{so}	Slot opening height	1.2mm
h_{wed}	Wedge height	1.2mm
h_{bi}	Back iron height	25mm
D_{slot}	Slot diameter	178mm

Table 3.3 illustrates the rotor design specification of SPM machine. But some information such as rotor external diameter at the airgap and shaft diameter are same for all machine. Value of Magnet thickness and magnet span are the same for SMPM and inset PMs Machines. Last Table 3.4 in this section discloses properties of material

Table 3.3: Design Specification for Rotor

Symbol	Parameters	Value
g	Air gap	0.7mm
D_{re}	Rotor external diameter at the air gap	158.6mm
D_{ri}	Shaft diameter	70mm
h_m	PM thickness	4mm
PPM	PM span	0.75

that have been used in designing rotor and stator in FEMM. These properties have been used to evaluate the various losses in machine both for analytical and FEMM analysis.

3.2 Description of Models

In this thesis four different rotor structure of PMSM to be simulated using FEMM and two different types of synchronous reluctance motors are to be created and analysed in FEMM. In the next section, a brief descriptions of each topologies are given before creating model in FEMM environment.

Table 3.4: Material Properties

Symbol	Parameters	Value
σ_{cu}	Copper conductivity at $120°C$	28MS/m
γ_{cu}	Specific weight of the iron	$7800kg/m^3$
P_{spec_fe}	Iron losses coefficient	2.3 W/kg
f_{ref}	Reference frequency for iron losses calculation	50Hz
B_{fe_ref}	Reference iron flux density for iron losses calculation	1T
k_{mag_t}	Teeth iron losses safety coefficient	2
k_{mag_bi}	Back iron losses safety coefficient	1.5

3.2.1 SMPM Machine

Nowadays Surface mount permanent magnet motor (SMPM) are widely used in the traction application. Most of the PMs Motors are the SMPM configuration motor. These are the synchronous motor where magnets are embedded in the surface of the rotor as shown in Figure 3-1. PMs are glued onto the rotor surface with the help of carbon and glass fibre bandage. Cogging torque can be reduced to a large extend by optimizing the magnet placing in the rotor surface. It is relatively a low cost PMs motors because the manufacturing of SMPM machine is very simple as a result their usage are increasing day by day.

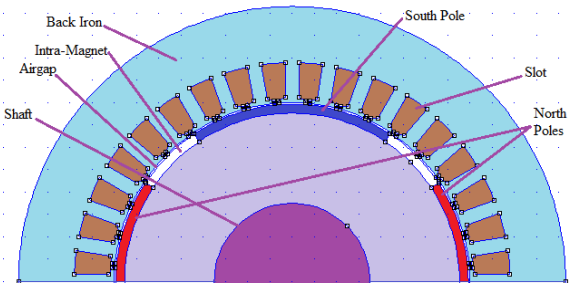

Figure 3-1: Schematic diagram of SMPM machine

However, it sometimes shows brittleness in the glued structure because of high centrifugal forces. This configuration has no saliency as stator current does not see the preferred magnetic direction meaning that equal permeability of air and magnet. Figure 3-1 shows sectional view of SMPM machine where north poles are in red coloured and south poles are in blue coloured. Intra-magnet is placed in between two

PMs in order to retain the magnets against high centrifugal forces and to make the structure robust.

3.2.2 Inset PMs Machine

In Inset PMs motor, PMs are magnetized in radially. It is shown in Figure 3-2, permanent magnet is placed onto rotor surface and embedded into shallow slots in order to protect against centrifugal force. Inset Permanent machine is more robust in structure which ensures better operation than its SPM counterparts. This configuration has large path in the rotor as result rotor iron saturation is achieved at higher currents. This motor shows saliency as q-axis reluctance is higher than d-axis reluctance.

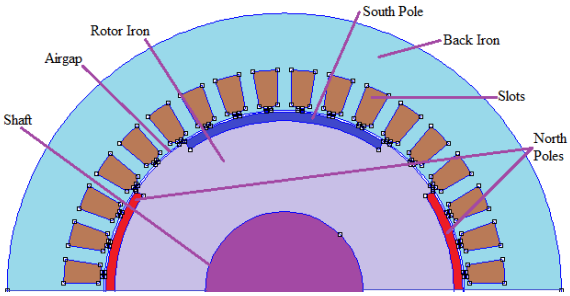

Figure 3-2: Schematic diagram of Inset PMs machine

3.2.3 Interior PMs Machine

Interior permanent magnet motors are very much compatible with extended speed range operation in the constant power region. It is a type of motor where permanent magnet is embedded in deep slots in the rotor as shown in Figure 3-3. This motor

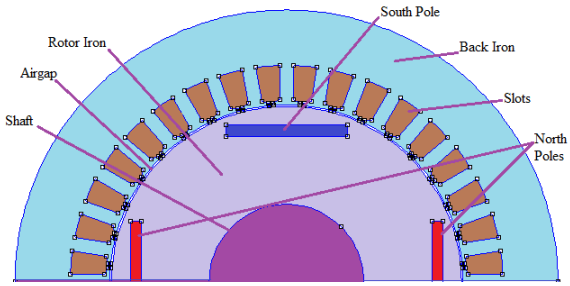

Figure 3-3: Schematic diagram of Interior PMs machine.

has freedom for embedding various rotor structures. It shows the saliency and the synchronous reactance in the q-axis is greater than that of d-axis. Buried magnet permanent magnet motor shaft is usually made with non ferromagnetic material. It reduces risk of being peeled off by centrifugal force. However, manufacturing is the cumbersome process which incurs higher production cost.

3.2.4 PMASR Machine

PMASR motors are formed by adding a PMs in each flux barrier of Synchronous reluctance motor as shown in Figure 3-4. Other than some PMs in the flux barrier, this machine is same as Synchronous reluctance motors in all respect. This additional PMs helps to get better torque, increases power factor and operational efficiency than Synchronous reluctance with a very low additional cost. It also offers cheap manufacturing and magnetisation process. Low cost ferrite magnet is good competitive choices in this particular machine.

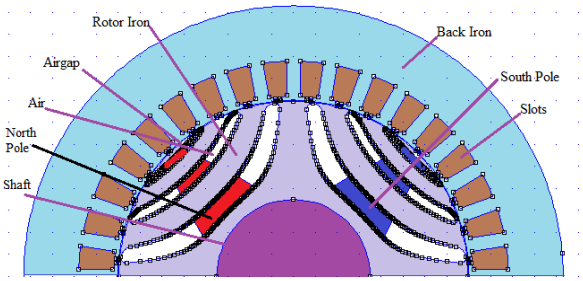

Figure 3-4: Schematic diagram of PMASR machine

3.2.5 SynR Machine

Figure 3-5 shows an axial view of four poles SynR motor with three flux barrier in each pole. Flux barrier serves to create specific flux path in the rotor and the flux lines flow in parallel to the flux barrier. Since this path is high permeability path is called d-axis. On the other hand, there is a low permeability path along through the flux barrier is called q-axis. Synchronous reluctance motors are continuously gaining attention because of its high torque density, high dynamic and fault tolerant capability. However, high torque ripple is the main draw backs of this machine.

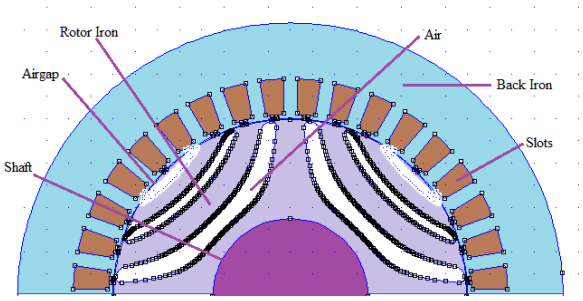

Figure 3-5: Schematic diagram of SYN REL machine

3.2.6 Segmented REL Machine

Segmented reluctance motor, also called Inverse reluctance motor, is new inclusion in synchronous reluctance motors. It is a machine without permanent magnet like synchronous reluctance motor. Only irons are used in the place of flux barrier region of synchronous reluctance machine as shown in Figure 3-6. All other parts of the rotor are constituted with non ferromagnetic material which has permeability close to air, that is why it is denoted by air in Figure 3-6. The shaft is also made of non ferromagnetic material. Segmented REL machine is low cost machine, however, their torque-speed performance is very poor.

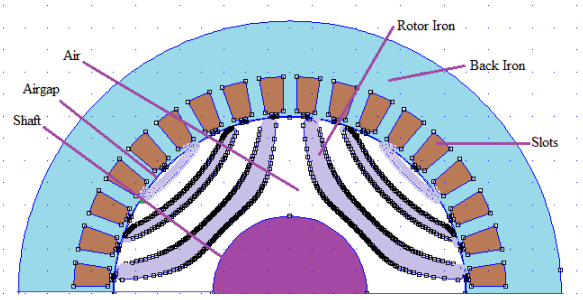

Figure 3-6: Schematic diagram of Segmented REL machine

3.3 Developing MATLAB Model

FEMM is very high powerful tool for analysing the linear or non linear magnetic problems in two dimensional planners. The idea of finite element analysis is to break the problem down into smaller areas then very simple functions can evaluate solutions of these areas. Principle is that smaller the problem area is the greater potentiality to

get precise answers. The main advantage of FEMM is that it is incorporated with Lua Scripting, a scripting language which is compatible with Matlab. Individual Matlab programs have been created to form each topology as shown in from Figure 3-1 to Figure 3-6. Each program consists of some calling functions with the aiming to do a specific work. For example, a function named 'data_motor' has been called at the starting of main file to get main geometrical data and parameters of the motors.

3.3.1 Creating Stator

A function is called in the main program for the purpose of creating stator geometry based on information provided by function 'data_motor'. A simple script is written to determine the eight points of each slot same as shown in Figure 3-7. Two commands 'Moverotate' and 'Copyrotate' were used to create 36 similar slots that employing in the whole circumference which means nine slots employ per pole. Another command has been called to add material in each slots and in the back iron core.

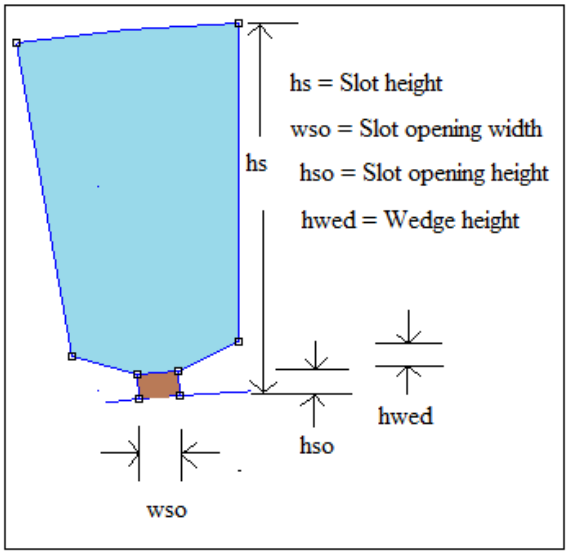

Figure 3-7: Axial view of a slot with some definitions of its lengths

3.3.2 Creating Rotor

Another function similar to stator creation function was also called in the main program for the purpose of creating rotor geometry based on information provided by

function 'data_motor'. Unlike stator part, rotor part and its geometry are different for individual models. Shaft geometry is also created in this function but shaft geometry is similar. Finally appropriate materials were inserted by selecting every block in rotor part.

3.4 Analysing Procedures

Once the whole model has been created successfully, then model is to be ready for analysing further. A script was written to determine the MTPA angle of each topology. The goal is to find the pairs of I_d and I_q current for which maximum torque is to be achieved with given phase current of 600Amps as stated earlier. After putting the determined MTPA angle in another script which calculates key electromechanical performance indicators with help of nested functions.

Chapter 4

Analytical Analysis of SMPM Machine

This chapter discusses analytical model of SMPM machine and its result will be analysed and compared with results of FEM.

4.1 Key Machine Performance Characteristics

This section calculates the key electromechanical performance parameters of SMPM machine analytically with air gap 0.7mm. Some assumptions need to be made in analytical analysis such as there is no either thermal, saturation, insulation issues nor rated performance issue.

4.1.1 Air Gap Flux Density Calculation

It is to be noted that airgap flux density is calculated here for no load condition. Air gap flux density can be calculated by using following formula

$$\hat{B_g} = \frac{B_{rem}.k_\sigma}{1 + \frac{g.k_{cart}.\mu_r.k_\sigma}{h_m}} \tag{4.1}$$

here,

B_{rem} = Remnant magnetic field density of ferrite

k_σ = Coefficient of pole span effect

k_{cart} = Carter coefficient

μ_r = Relative permeability of ferrite

The coefficient for pole span effect, k_σ, is expressed as

$$k_\sigma = \frac{\tau_p}{\tau_p + 2g} \tag{4.2}$$

where,

τ_p = Pole pitch

Pole pitch,τ_p, is defined as distance between centre to centre of two adjacent magnetic pole, which covers 180 electrical degree can be written as follows

$$\tau_p = \frac{\pi D_s}{2p} \tag{4.3}$$

After putting the values in equation (4.3), then we obtain

$$\tau_p = \frac{\pi \times 0.1586}{2 \times 2} = 0.125m$$

After putting the values in equation (4.2), then we get value of cofficient of pole span effect is

$$k_\sigma = \frac{0.125}{0.125 + 2 \times 0.7 \times 10^{-3}} = 0.988$$

The carter coefficient can be obtained as follows

$$k_{cart} = \frac{\tau_u}{\tau_u + g - \frac{3}{4} wso} \tag{4.4}$$

where,

τ_u = Slot pitch

If there are Q_s slots in the stator, slot pitch can be calculated by dividing the air gap periphery by the slot number.

$$\tau_u = \frac{\pi D_s}{Q_s} \tag{4.5}$$

According to equation (4.5), value of slot pitch is

$$\tau_u = \frac{\pi \times 0.16}{36} = 0.014$$

So from equation (4.4), we get the value of carter coefficient is

$$k_{cart} = \frac{0.014}{0.014 + 0.7 \times 10^{-3} - \frac{3}{4} \times 2 \times 10^{-3}} = 1.06$$

Now, we obtained airgap flux density is

$$\hat{B_g} = \frac{0.35 \times 0.988}{1 + \frac{0.7 \times 10^{-3} \times 1.06 \times 1 \times 0.988}{4 \times 10^{-3}}} = 0.292T$$

Now average flux per pole can be calculated by the following equation

$$\hat{\Phi} = \frac{\hat{B_g} D_s L_{stk}}{poles} \tag{4.6}$$

After putting the values in equation (4.6), then we get the value of average flux per pole is

$$\hat{\Phi} = \frac{0.292 \times 0.160 \times 0.220}{4} = 2.57 \times 10^{-3} Webers$$

4.1.2 Torque Calculation of SMPM Motor

Torque can be estimated by the following equation

$$T = \frac{\pi}{2} k_w D_{re}^2 L_{stk} BA = 2BVA \tag{4.7}$$

where,

B = Magnetic loading

A = Electric loading

V = Volume of the motor

Electrical loading is determined as a function of rated current as

$$A = \frac{Q_s n_c I}{\pi D_{re}} \tag{4.8}$$

After putting the all values in equation (4.8), then we get the value of electric loading

$$A = \frac{36 \times 1 \times \frac{600}{\sqrt{(2)}}}{\pi \times 0.1586} = 30653.89 A/m$$

Since the motor is in cylindrical shape, so volume of motor can be calculated by the following formula as

$$V = \pi \left(\frac{D_{re}}{2}\right)^2 L_{stk} \tag{4.9}$$

So, the volume of the motor is

$$V = \pi \left(\frac{0.1586}{2}\right)^2 \times 0.220 = 4.346 \times 10^{-3} m^3$$

Now, torque can be calculated by putting the value in equation(4.7), we get

$$T = 2 \times 0.292 \times 4.346 \times 10^{-3} \times 30653.89 = 77.80 Nm$$

4.2 Loss Calculation

This section evaluates the different loss of SMPM machine. In the first part of this section estimates the Copper loss and second part calculates the Iron loss.

4.2.1 Copper loss calculation of SMPM motor

Copper loss can be calculated by equations (2.37) and (2.38) as stated in previous chapter.

The lengths of the copper conductor is estimated by the following formula as

$$l_{ew} = \pi \frac{\tau_u}{2} \tag{4.10}$$

After putting the all values in equation (4.10), then we get the lengths of the copper conductor is

$$l_{ew} = \pi \frac{0.014}{2} = 21.99 \times 10^{-3} m$$

Number of conductors per phase, N_{ph}, can be calculated as follows

$$N_{ph} = \frac{Q_s n_c}{a \times m} \tag{4.11}$$

here,

a = Number of parallel circuits per phase

m = Number of phases

So, number of conductor per phase is

$$N_{ph} = \frac{36 \times 1}{1 \times 3} = 12$$

Cross-section of copper conductor, S_{cu}, is calculated as follows

$$S_{cu} = S_{slot} \times k_{fill} \tag{4.12}$$

Cross section of copper conductor values is calculated

$$S_{cu} = 155.1226 \times 10^{-4} \times 0.4 = 6.20 \times 10^{-3} m^3$$

After putting the all variable values in equation (2.37), Copper resistance per phase can be calculated as

$$R = 28 \times 10^{-6} \frac{12\,(0.220 + 21.99 \times 10^{-3})}{6.20 \times 10^{-3}} = 13.11 \times 10^{-3} \Omega$$

Electric loading as a function of torque and air gap flux density is expressed as:

$$k_s = \frac{2T}{\pi D_s^2 L_{stk} \hat{B}_g} \tag{4.13}$$

Electric loading can be calculated as from equation (4.13)

$$k_s = \frac{2 \times 77.80}{\pi \times 0.16^2 \times 0.220 \times 0.292} = 30117.174 A/m$$

Electric loading for 3-phase machine is

$$k_s = \frac{6 I_n N_{ph}}{\pi D_{re}} \tag{4.14}$$

Phase current, I_n, can be expressed as a function of electrical loading k_s

$$I_n = \frac{\pi D_{re} k_s}{6 \times N_{ph}} \tag{4.15}$$

After putting the all values in equation (4.15), then we get phase current is

$$I_n = \frac{\pi \times 0.1586 \times 30117.174}{6 \times 12} = 208.42 A$$

Now putting the all values in equation(2.37), so total copper loss

$$P_j = 3 \times 13.11 \times 10^{-3} \times 208.42^2 = 1708.42 W$$

4.2.2 Iron loss calculation of SMPM motor

Electrical frequency of the motor can be calculated for motor base speed of $3000rpm$ by the synchronous speed equation.

$$n_s = \frac{120 f_{elect}}{poles} \tag{4.16}$$

So, electrical frequency of the machine is

$$f_{elect} = \frac{n_s \times poles}{120} = \frac{3000 \times 4}{120} = 100Hz$$

Specific losses per kg at the tooth under given condition can be determined as

$$P_{spec\_t} = 2.3 \times (B_{t\_max})^2 \times \left(0.7 \times \frac{f_{elect}}{50} + 0.3 \times \left(\frac{f_{elect}}{50}\right)^2\right) \tag{4.17}$$

Tooth magnetic field density of SMPM motor is calculated of 1.58 T using FEM as shown in Figure 5-4 and value of back iron flux density is recorded of 0.94 T.

Specific losses per kg at the tooth is

$$P_{spec\_t} = 2.3 \times (1.58)^2 \times \left(0.7 \times \frac{100}{50} + 0.3 \times \left(\frac{100}{50}\right)^2\right) = 14.93W/kg$$

The weight of the tooth is calculated by the following formula

$$Pseo_t = \gamma_{fe} \times Q_s \times h_s \times w_t \times L_{stk} \tag{4.18}$$

So, the total weight of tooth is

$$Pseo_t = 7800 \times 36 \times 0.018 \times 6.2 \times 10^{-3} \times 0.220 = 6.895kg$$

The iron losses in the tooth can be calculated by the following formula

$$P_{fe\_t} = k_{magg\_t} \times P_{spec\_t} \times Peso_t \tag{4.19}$$

After putting the all values in equation(4.19), we get

$$P_{fe\_t} = 2 \times 14.93 \times 6.89 = 205.74Watts$$

Specific losses per kg at the back iron under given condition

$$P_{spec\_bi} = 2.3 \times (B_{bi\_max})^2 \times \left(0.7 \times \frac{f_{elect}}{50} + 0.3 \times \left(\frac{f_{elect}}{50}\right)^2\right) \tag{4.20}$$

After putting the all values in equation(4.20), we get specific losses per kg at back iron is

$$P_{spec\_bi} = 2.3 \times (0.94)^2 \times \left(0.7 \times \frac{100}{50} + 0.3 \times \left(\frac{100}{50}\right)^2\right) = 5.28W/kg$$

The weight of the back iron can be calculated by the following formula

$$Pseo_{bi} = \gamma_{fe} \times \pi \times (D_e - h_{bi}) \times h_{bi} \times L_{stk} \tag{4.21}$$

Total weight of the back iron is

$$Pseo_{bi} = 7800 \times \pi \times (0.246 - 0.025) \times 0.025 \times 0.220 = 29.785Kg$$

The iron losses in the back iron is calculated by the following formula

$$P_{fe\_bi} = k_{magg\_bi} \times P_{spec\_bi} \times Peso_{bi} \tag{4.22}$$

After putting the all values in equation(4.20), we obtain iron losses in the back iron

$$P_{fe\_bi} = 1.5 \times 5.28 \times 29.785 = 235.90Watts$$

Total iron losses

$$P_{fe} = 205.74 + 235.90 = 441.64Watts$$

4.2.3 Efficiency Calculation of SMPM motor

Total losses in motor

$$P_l = 1708.42 + 441.64 = 2150.06Watts$$

Output power of the motor is calculated as

$$P_{out} = T \times \omega \tag{4.23}$$

Mechanical speed, ω, in radian is expressed as

$$\omega = 3000 \times \frac{2\pi}{60} = 314.16 rads^{-1}$$

Now putting the value in equation(4.23), then we obtain the total output power of the machine is

$$P_{out} = 77.80 \times 314.16 = 24.44kW$$

Efficiency can be calculated as

$$\eta = \frac{24.44 \times 10^3}{24.44 \times 10^3 + 2150.06} \times 100\% = 91.91\%$$

4.2.4 Induced Voltage of SMPM Motor

Phase induced voltage in AC rotating machine is expressed as

$$E_{ph} = \sqrt{2} \times \pi \times f_{elect} \times \Phi \times N_{ph} \times k_w \tag{4.24}$$

here,

Φ = Average flux

k_w = Winding factor

So, induced e.m.f per phase is

$$E_{ph} = \sqrt{2} \times \pi \times 100 \times 2.57 \times 10^{-3} \times 12 \times 1 = 13.70V$$

4.3 Comparison with FEMM Results

This section compares the analytical model results with FEMM model results. Table 4.1 illustrates dependencies of key electromechanical performances between analytical and FEM model results.

It is noticeable that value of torque, copper loss, iron loss, airgap magnetic flux density and output power of analytical model are greater than FEM. On the other hand, efficiency and average flux show the opposite trends.

Value of torque of analytical model is 15.85 percent higher than FEMM model. Efficiency of FEMM results is higher though torque is lower than analytical model,

Table 4.1: Comparison of Analytical Results with FEMM Results

Particulars	Unit	Analytical Results	FEMM Results
Torque	Nm	77.80	67.15
Copper Loss	Watts	1708.42	1146.90
Iron Loss	Watts	441.64	389.16
Efficiency	%	91.91	93.36
Average Flux	Webers	2.58×10^{-3}	7.44×10^{-3}
Airgap Magnetic Flux Density	T	0.292	0.27
Output Power	Watts	24.44×10^{3}	21.09×10^{3}

this is because of higher losses in analytical model. It is noticeable that copper loss in analytical model is 48.95% higher than FEMM model.

The difference in values between analytical and FEMM models in case of efficiency and airgap magnetic flux density are pretty close.

Chapter 5

Analysis of FEMM Results of PMSM Machine

In this chapter, FEMM results of first four configurations of PMs Machines are investigated based on design procedure discussed in earlier chapter. This chapter examines the following points about the performance of studied configurations.

- Calculation of MTPA angle of each topology
- Showing the behaviour of torque
- Representation of losses
- d- and q-axis flux linkage
- d- and q-axis inductances and their saliency ratio
- flux density map showing saturation of magnetic flux in particular area
- Air gap flux density plot
- Repeat the above measurements with reduced airgap model

5.1 Analysis of SMPM machine

This section evaluates solely the performance of SMPM machine. The investigation is carried out for $0.7mm$ of air gap.

5.1.1 Finding MTPA Angle of SMPM Motor

A code is written to find out maximum torque for different angle of current vector in d-q reference frame. Phase current is set to $600Amps$ and varies the current angle from 0 to 180 degree with step size of 2 degree; torque has been recorded at every increment. The torque is then plotted as function of current angle and corresponding graph as shown in Figure 5-1. It is clearly seen from the graph that

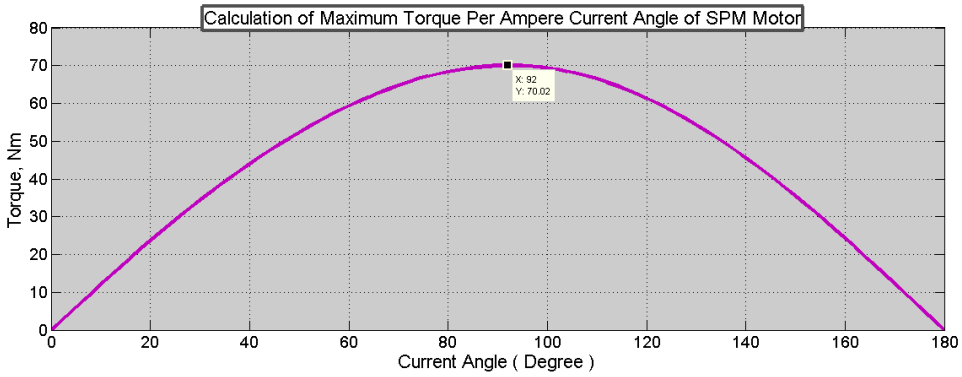

Figure 5-1: Calculation of maximum torque per ampere current angle of SMPM machine

the maximum torque is $70Nm$ at $92degree$ where I_d and I_q are $-20.94Amps$ and $599.63Amps$ respectively. In theory SMPM machine is a non salient machine but in practice shows very little saliency, this is due to saturation of magnetic field.

5.1.2 Calculation of Performance Parameters

By setting the MTPA current angle, another simulation is carried out to evaluate the key performance parameters such as torque, flux linkage both in ABC and d-q reference frame, force, energy and co-energy and losses. Data has been recorded over the rotation of the rotor in every mechanical degree up to 45 degree mechanical. Figure 5-2 is drawn by plotting the torque as a function of mechanical angle of rotor. As is illustrated by the graph, there is a steady state deviation of torque from average torque is of $67.16Nm$ so torque ripple is about 16%.

Different losses of SMPM machine with the air gap of $0.7mm$ is shown in Figure 5-3. It can be seen from the graph, much more losses are incurred due to copper loss in comparison with iron loss. So, the total loss of SMPM machine on average is

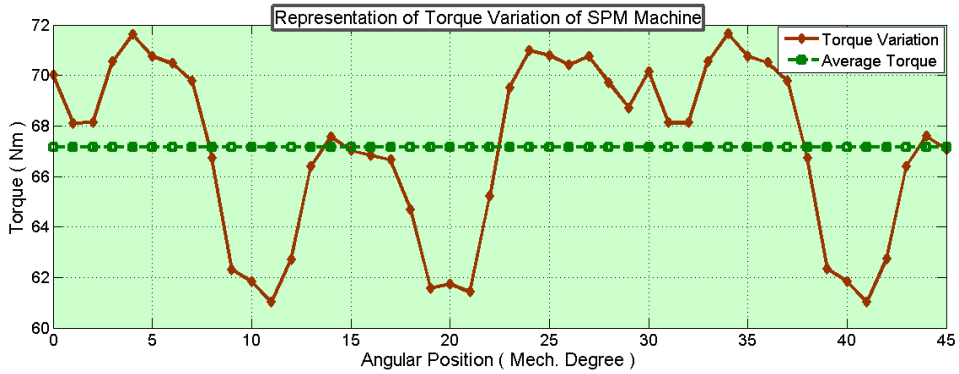

Figure 5-2: Behaviour of torque with respect to angular position of SMPM machine

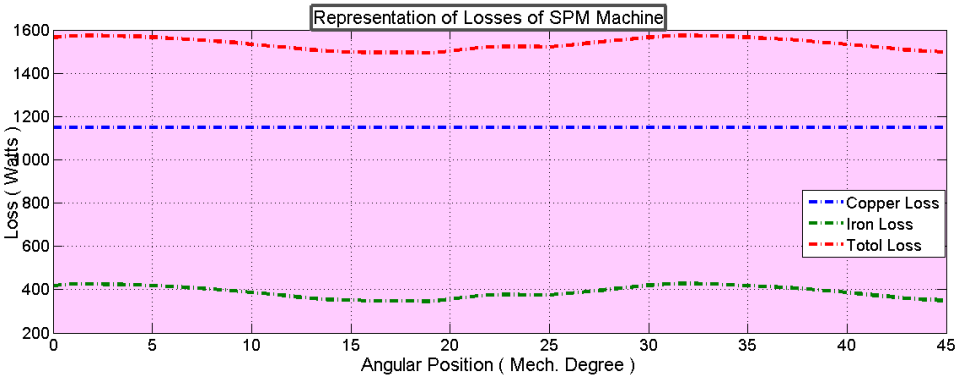

Figure 5-3: Measured different losses of SMPM machine

1536.07$watts$.

5.1.3 Density Map of SMPM Machine with Air-gap 0.7mm

Density plot of SMPM machine is shown Figure 5-4 with the air gap of 0.7mm. Resultant flux lines are seen fairly distributed throughout stator and rotor of the machine. The maximum value of flux density corresponding to teeth is measured of 1.58T. Similarly in back iron core and air gap maximum flux density are 0.94T and 0.67T, respectively.

Normal component of average flux per pole of SMPM motor with air gap 0.7mm is of 0.0074$Webers$. A contour around the semicircle is drawn through the airgap in the post-processing mode of FEMM by selecting the contour mode toolbar. Magnitude of the air gap magnetic flux density plot has been drawn for the contour as shown in Figure 5-5. The prominent effect on magnetic field distribution is caused by slot which results of the effect appears as a spike in Figure 5-5.

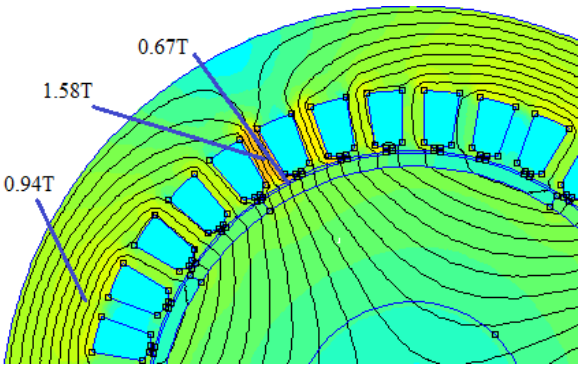

Figure 5-4: Flux density of plot of SMPM machine with airgap $0.7mm$

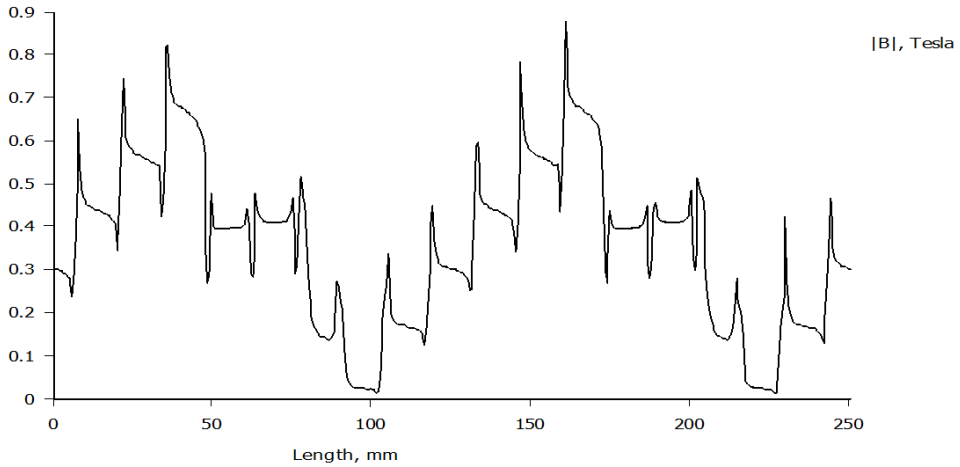

Figure 5-5: Airgap flux density of SMPM machine with airgap $0.7mm$

5.1.4 Flux Linkage of SMPM Machine with Air-gap 0.7mm

As shown in Figure 5-6, there are two lines conveying the information about flux linkage where dark red line represents d-axis flux linkage and green line denotes for q-axis flux linkage. Graphs are drawn corresponding to their I_d and I_q currents. Q-axis flux linkage graph shows linearity with respect to I_q but d-axis shows saturation for higher current. Q-axis flux linkage start from origin in contrast d-axis starts approximately at $0.03web - t$, this is because of presence of magnet flux in the direct axis.

5.1.5 Inductances and Saliency Ratio

As can be seen from the Figure 5-7, inductance of d-axis and q-axis of SMPM machine with air gap $0.7mm$ is equal up to stator current $300Amps$. In practice,

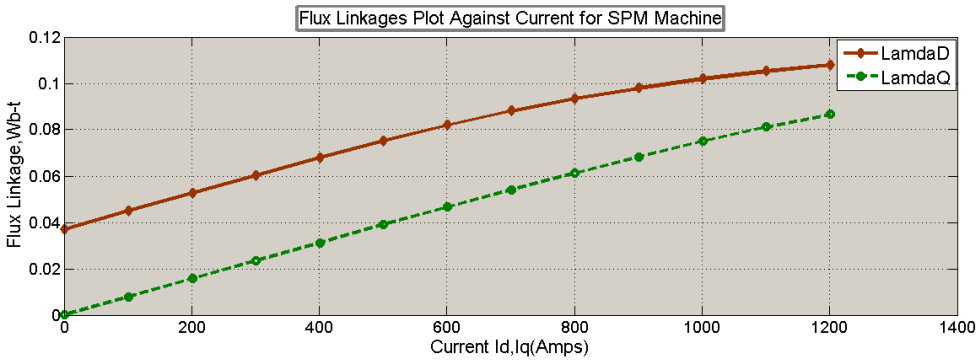

Figure 5-6: Plot of d- and q-axis flux linkage vs. Current of SMPM machine

predicted magnitude of L_d should be equal to magnitude of L_q for any currents since it is a non - salient machine. However, the magnitude of L_d has been decreased after the saturation occurs in d-axis at current $300Amps$. Saliency ratio is measured as

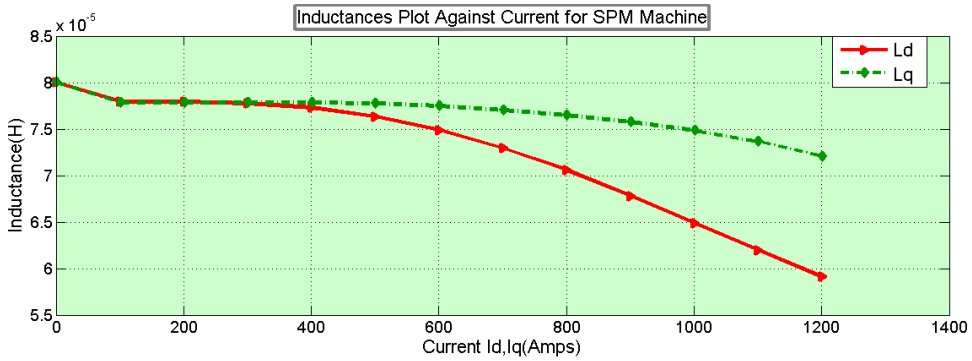

Figure 5-7: Measured inductances as a function of current of SMPM machine

ratio of d-axis inductance over q-axis inductance. Figure 5-8 shows the saliency ratio of SMPM machine with air gap $0.7mm$. From the graph it is clear that saliency ratio is equal to 1 up to $300Amps$. Saliency ratio is started to decrease after the current values of $300Amps$ and its lowest value is calculated of 0.82 at current $1200Amps$.

5.2 Optimization of SMPM Machine

Another FEM model of SMPM machine has been created with half of the air gap of previous model but all other structures are being kept identical. All the simulations are carried out to get key performance parameters. Each of the following sections compares and contrasts the results of both topologies.

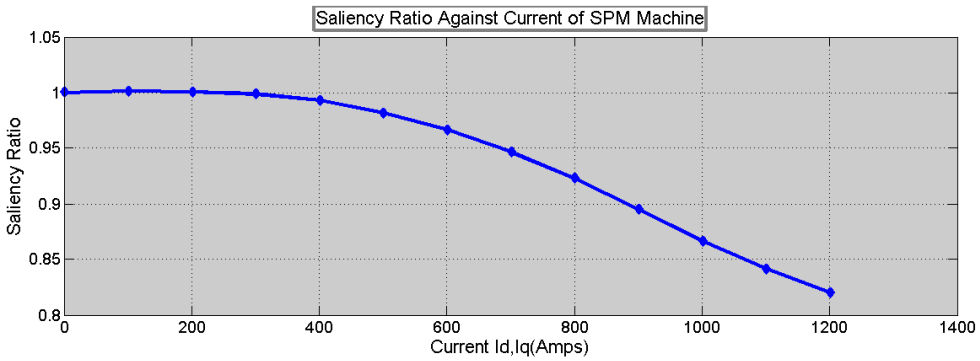

Figure 5-8: Saliency ratio (Ld/Lq) as a function of current of SMPM machine

5.2.1 Comparison of MTPA Angle

Torques from both models is plotted as a function of current angle in the same graph is shown in Figure 5-9. It is clearly seen from the graph, there is a significant increase in torque for per ampere current angle of SPM machine with the air gap 0.35mm than air gap model of $0.7mm$. The maximum torque is also calculated of

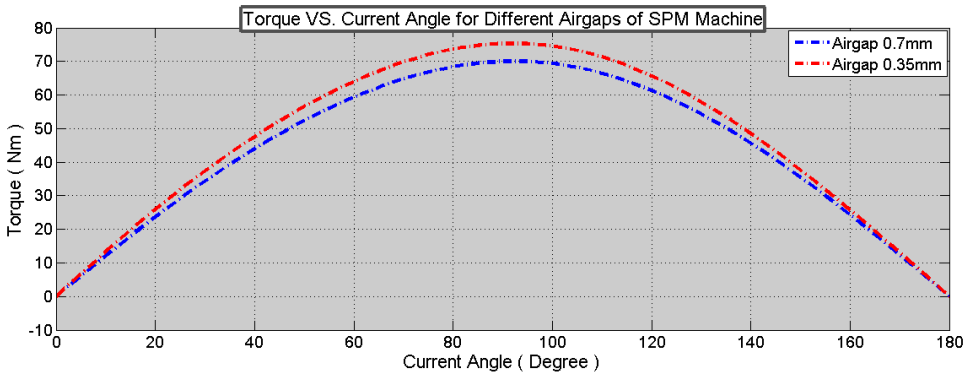

Figure 5-9: Plot of torque vs. Current angle for two different air gaps in SMPM machine

$75.33Nm$ at $92degree$ where I_d and I_q currents are $-20.94Amps$ and $599.64Amps$, respectively. This increment of maximum torque would represent approximately 7.61% of previous model with air gap $0.35mm$ at MTPA angle.

5.2.2 Comparison of Performance Parameters

Comparison of torque variation between two air gaps models of SMPM machine is shown in Figure 5-10. Torque is calculated for one degree mechanical rotation of

rotor. There is a slight increase in torque in model with air gap 0.35mm than air gap model 0.7mm at every rotor position. The average torque for new model is measured

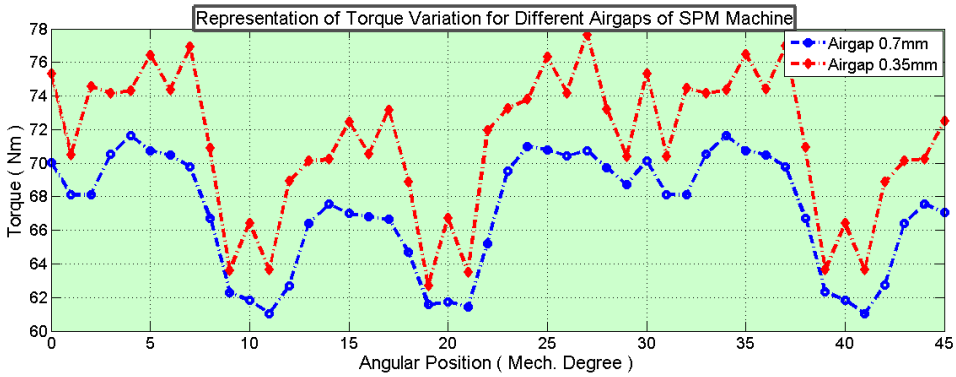

Figure 5-10: Comparison torque variation with respect to angular position for two different air gaps in SMPM machine

of 71.34Nm which is accounted for 6.23% increase from previous model. Efficiency of SMPM motor with air gap 0.35mm is varied over the different angular position of rotor. Efficiency of SPM with air gap 0.35mm motor is shown in Figure 5-11. Average

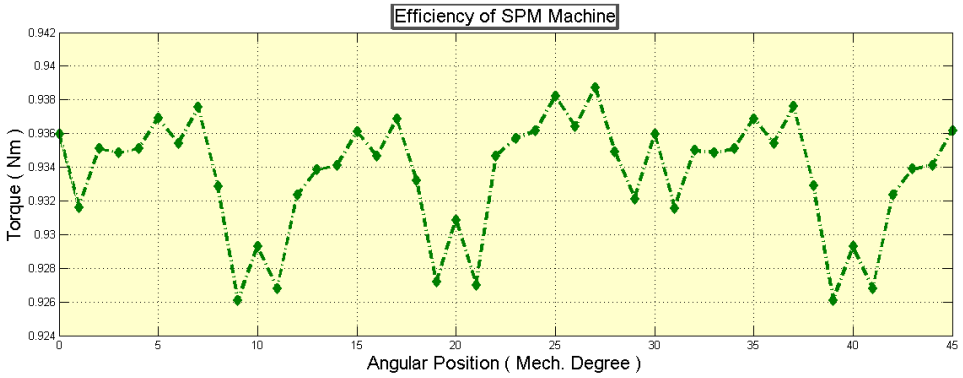

Figure 5-11: Measured of efficiency of SMPM machine with airgap 0.35mm

efficiency of SMPM motor is 93.36% where the maximum efficiency is estimated of 93.87% at rotor position of 27 degree mechanical.

5.2.3 Density Map of SMPM Motor with Air Gap 0.35mm

Density map of SMPM machine with the air gap 0.35mm is shown in Figure 5-12. This density mapping has been executed by applying the 600$Amps$ current in the stator circuit while position of rotor was 1 mechanical degree. As is illustrated by the

density map, magnetic flux lines generated around the rotor as well stator for reduced air gap SMPM machine are more than 0.7mm air gap model. Maximum magnitude

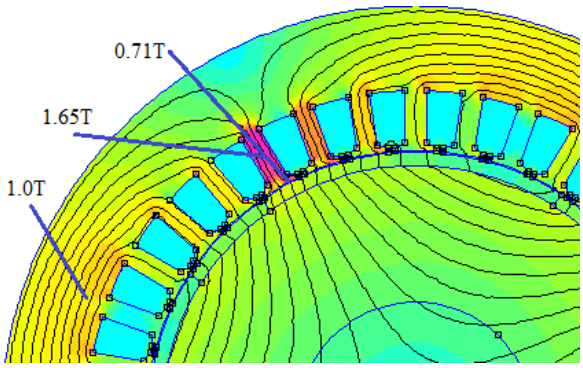

Figure 5-12: Flux density of plot of SMPM machine with airgap $0.35mm$

of flux density of teeth has increased to $1.65T$. Similarly, other places such as back iron core and air gap are found to more fluxes and their values are $1.0T$ and $0.71T$ respectively. A contour covers half circle through the air gap is drawn in order to

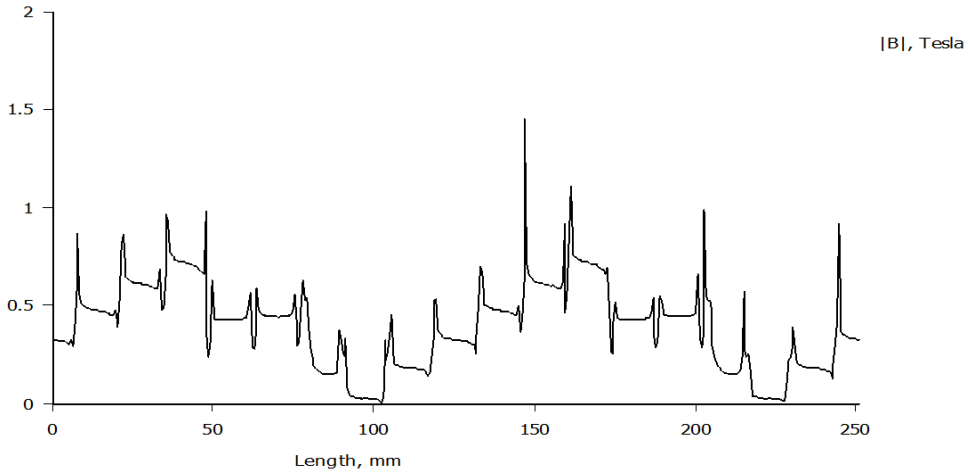

Figure 5-13: Airgap flux density of SMPM machine with airgap $0.35mm$

examine behaviour of air gap flux density. Air gap flux density of SMPM machine with air gap is shown in Figure 5-13. Like previous model slotting effect are also prominent in this Figure 5-13. Normal component of average flux per pole of SMPM motor with airgap $0.35mm$ is measured as $0.0080Webers$.

5.2.4 Summary of Comparison

Table 5.1 summarize the main electromechanical results such as average torque, average total loss, torque ripple, average d-axis flux linkage, average q-axis flux linkage and efficiency for both models. It is noticeable that all the parameter value for air gap $0.35mm$ are strikingly higher than the model with air gap $0.7mm$. However, ripple has been increased by 30 percent.

Table 5.1: Comparison of Optimized Results with Base Model of SMPM Motor

Parameters	Unit	Airgap $0.7mm$	Airgap $0.35mm$
Average Torque	Nm	67.16	71.34
Average Total Loss	Watts	1536.067	1590.17
Ripple	%	15.80	20.93
Efficiency	%	93.21	93.38

5.3 Analysis of Inset PMs Machine

This section describes details how to analyse the model and provides the information about electromechanical characteristics of Inset PMs machine with air gap $0.7mm$.

5.3.1 Finding MTPA angle of Inset PMs Motor

A program is used to calculate maximum torque by varying the phase of current angle of Inset PMs motor. Maximum torque is achieved at current angle of $136degree$ is shown in Figure 5-14. Which means advance angle of this machine is $46degree$. Larger is the advance angle greater the negative I_d current. So, resulting I_d and I_q currents are $-431.60Amps$ and $416.80Amps$ respectively. It is worth noting that some negative torques values are observed for some initial phase current angles and these values are discarded when plotting the torque with respect to current angle.

5.3.2 Calculation of Electromechanical Performance of Inset PMs with Air Gap 0.7mm

Key electromechanical performances parameters are evaluated with the help of a program where phase current is fixed to $600Amps$ with current angle at $136degree$.

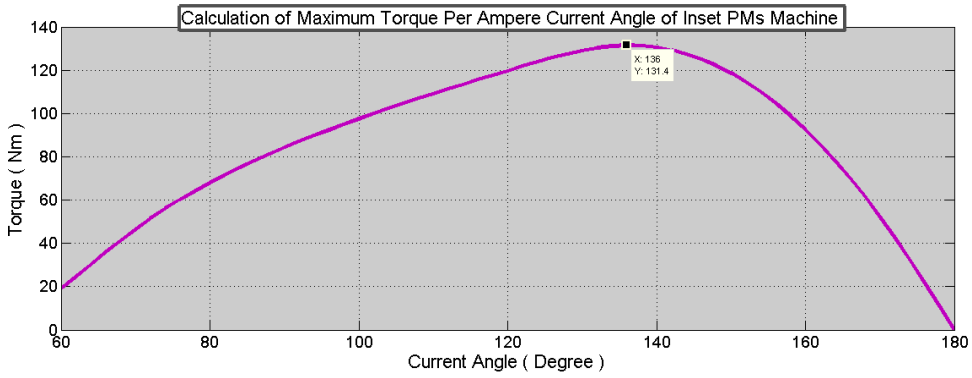

Figure 5-14: Calculation of maximum torque per ampere current angle for Inset PMs machine

A loop was carried out up to $45degree$ of mechanical rotation of rotor. Figure 5-

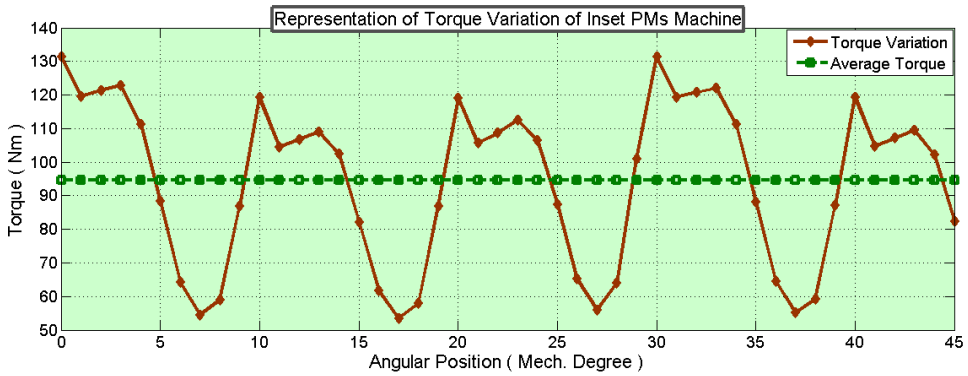

Figure 5-15: Behaviour of torque with respect to angular position of Inset PMs machine

15 shows the torque variation of Inset PMs machine with air gap $0.7mm$. It can be seen from the graph there is a significant fluctuation in the magnitude of torque. Average torque of this machine is estimated of $94.61Nm$. Maximum value of torque is found $131.40Nm$ at 0 degree and minimum value $53.33Nm$ at $17degree$ of mechanical rotation of rotor. There is huge gap between minimum and maximum values, as a result higher torque ripple is found as 82.51%.

Figure 5-16 shows the different losses of Inset PMs machine with air gap of $0.7mm$. There is no copper loss in the rotor since it is a PMs machine requires no current for magnetization. Copper loss is calculated as same as SMPM machine since both have identical stator structure. But average total loss of this machine is $1733.87watts$ which is a bit higher than SMPM machine with similar air gap.

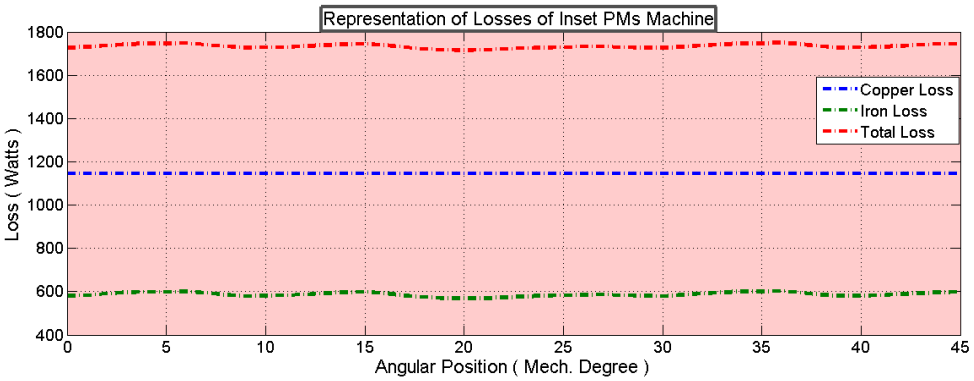

Figure 5-16: Measured different losses of Inset PMs machine

5.3.3 Density Map of Inset PMs Motor with Air Gap 0.7mm

A full load analysis is performed in order to show the flux level at different parts of the machine. Resultant flux lines are illustrated in Figure 5-17. The density

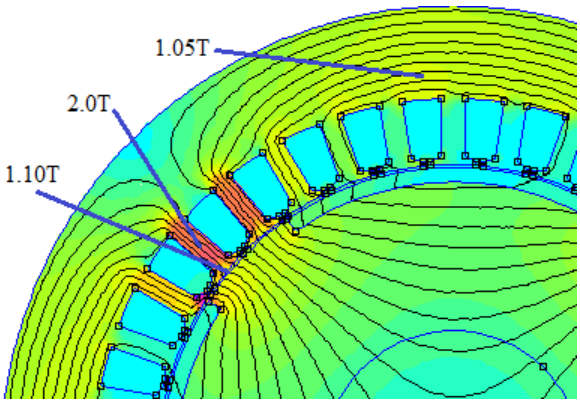

Figure 5-17: Flux density of map of Inset PMs machine with airgap 0.7mm

map shows local saturation corresponding to the area stator teeth and back iron. Maximum flux density of stator teeth and back iron are reported as $2.0T$ and $1.05T$, respectively.

Air gap flux density plot is presented in Figure 5-19. This contour plot has been drawn for semicircle through the air gap. An important slotting effect is also prominent in this Figure 5-19. Normal component of average flux per pole is reported $0.010Webers$.

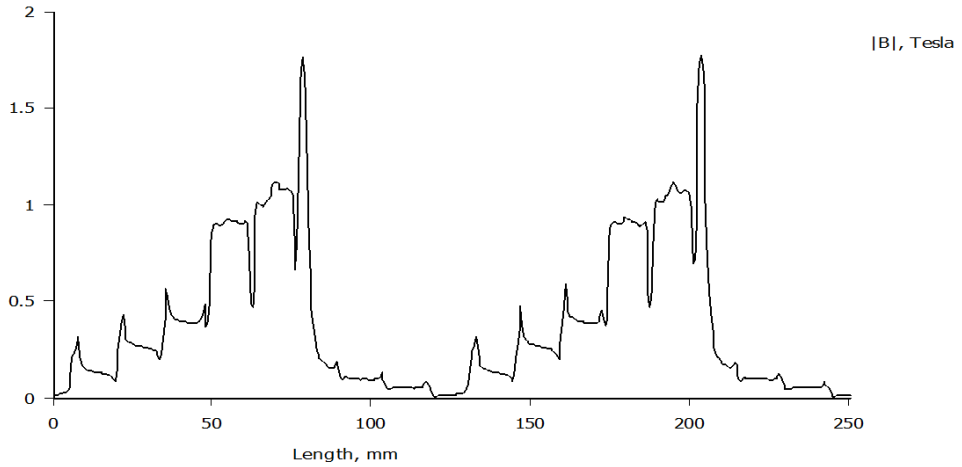

Figure 5-18: Air gap flux density plot of Inset PMs machine with air gap 0.7mm

5.3.4 Flux Linkage of Inset PMs Machine with Air-gap 0.7mm

Simulations are carried out to estimate the flux linkage along the d-axis and q-axis as well. Figure 5-19 shows the flux linkages as a function of I_d and I_q currents. More

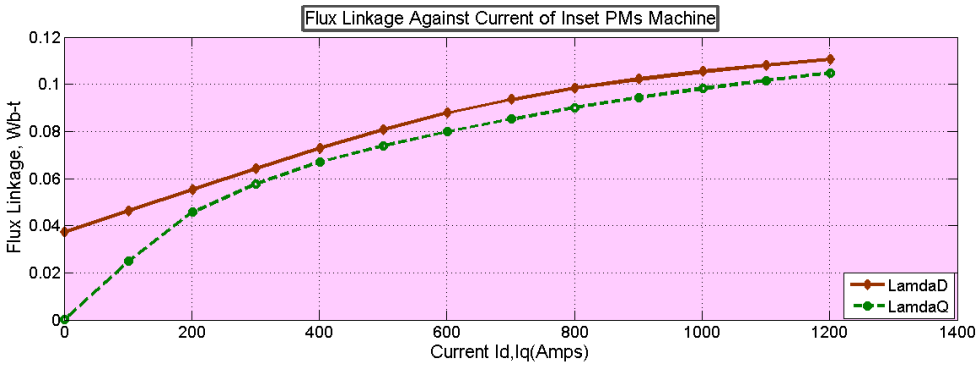

Figure 5-19: Plot of d- and q-axis flux linkages vs. Current in Inset PMs machine

flux linkages in d-axis than q-axis are reported for entire currents. A value of flux linkage along d-axis was found even without applying any stator I_d, current. This is because the presence of magnet fluxes Ψ_m is equal to $0.037Wb - t$ along the d-axis.

5.3.5 Inductances and Saliency Ratio

In order to be able to explain qualitative descriptions of Inset PMs at different operating points, d-axis and q-axis inductance calculation were performed. Figure 5-20 indicates the d and q axis inductances of inset PMs motor with air gap $0.7mm$. The

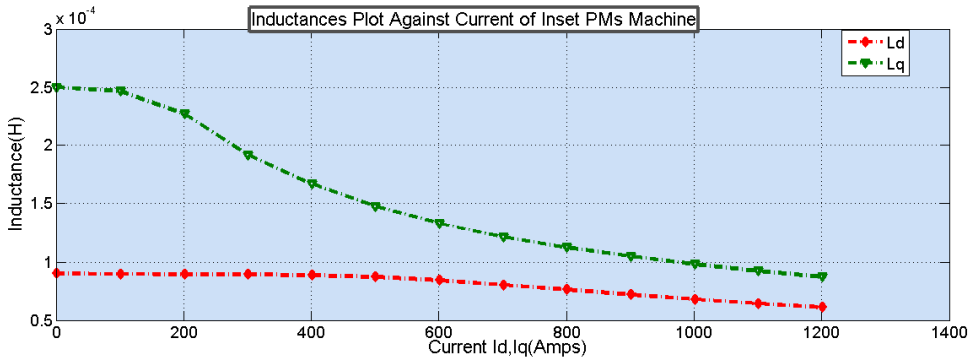

Figure 5-20: Measured inductances as a function of current of Inset PMs machine

graph depicts that for all values of currents there are more values of d-axis inductance than in q-axis inductance. The gap in values between d-axis and q-axis is decreasing with the increasing of current. Corresponding saliency ratio (L_d/L_q) graph is shown in Figure 5-21.

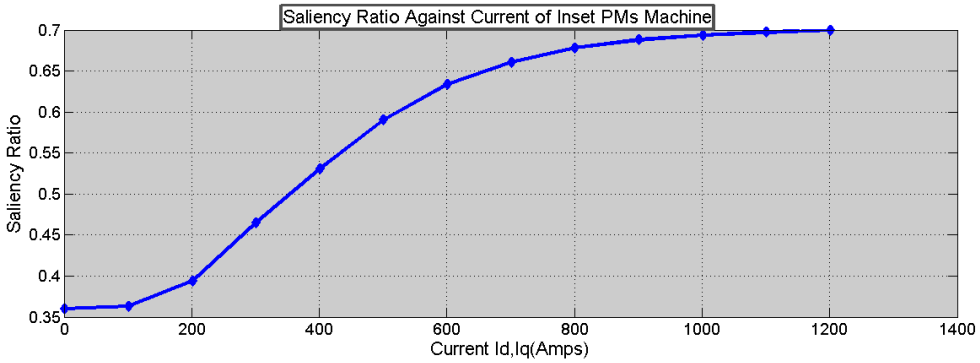

Figure 5-21: Saliency ratio (L_d/L_q) as a function of current of Inset PMs machine

It can easily be seen that saliency ratio is increased with increasing applied current. Which means that rate at decreasing the value of q-axis inductance is higher than in d-axis inductance with the increasing current. Maximum saliency ratio is reported of 0.7 at $1200 Amps$ of currents.

5.4 Optimization of Inset PMs motor

In order to optimize the motor performance another FEM model with reduced air of $0.35mm$ has been created. Several similar simulations have been carried out to examine the performance parameters. Following sections compare and contrast the

results of new model with old model.

5.4.1 Comparison of MTPA Angles

A simulation was carried out in order to calculate maximum torque by varying the current angle while phase current is set to $600 Amps$. Torques from both models are plotted with respect to angle of phase current and obtained graph is shown in Figure 5-22. As is shown by the graph that red line represents torque corresponds to air gap $0.35mm$ which has reached peak at $142 degree$. It is clearly seen that position of MTPA angle is shifted to the right by $6 degree$ with influence of reduced air gap.

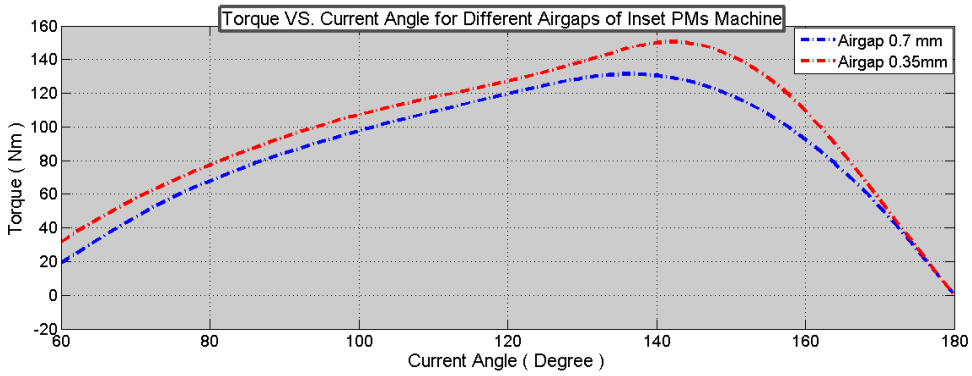

Figure 5-22: Plot of torque vs. Current angle for two different air gaps in Inset PMs machine

5.4.2 Comparison of Performance Parameters

Torque behaviour of Inset PMs motor with air gap $0.35mm$ is evaluated by means of FE analysis, moving the rotor of $45 degree$ mechanical. Comparison of torque variation of between two models is reported in Figure 5-23. As is illustrated by the graph maximum value of torque is reported of $150.46Nm$ where minimum value is only $39.12Nm$ which yields very high torque ripple of 109.90%. There is a less fluctuation in efficiency curve of Inset PMs motor with air gap of $0.35mm$ is seen in Figure 5-24. Average efficiency is recorded of 93.92% while minimum and maximum efficiency are 96.45% and 87.58%, respectively.

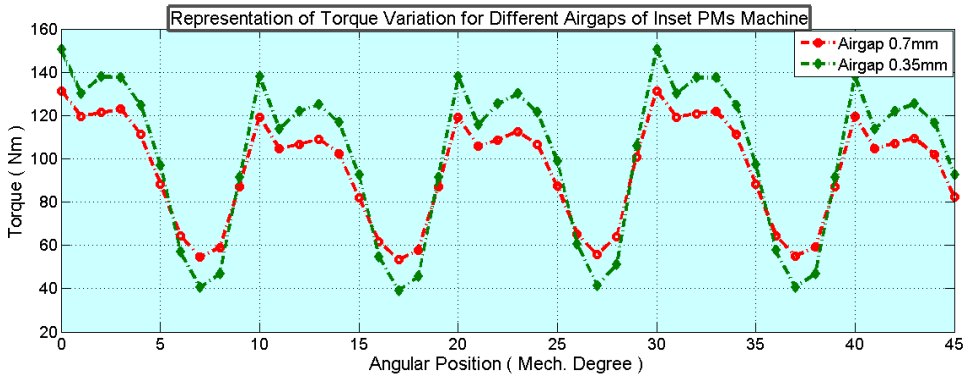

Figure 5-23: Comparison of torque variation with respect to angular position for two different airgaps of Inset PMs machine

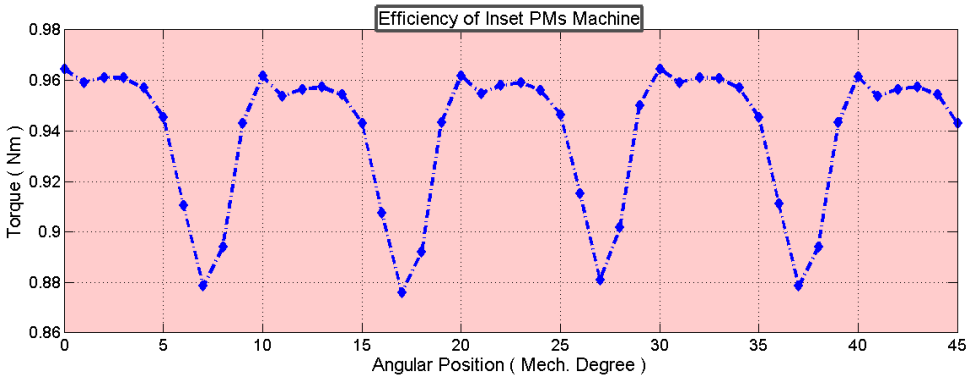

Figure 5-24: Measured efficiency of Inset PMs machine

5.4.3 Density Map of Inset PMs Motor with Air Gap 0.35mm

As expected, resultant flux lines of optimized design is shown in Figure 5-25 where saturation is observed in area corresponding to stator teeth. There is no significant influence of air gap on flux density. As can be seen from both density maps, very little increase in value of maximum flux density of back iron and air gap are $1.06T$ and $1.20T$, respectively. Air gap flux density plot is drawn in Figure 5-26 in post processing phase of FEM through the air gap. Flux density waveform shows rotor losses and slotting effect. Normal component of average flux per pole of Inset PMs motor with air gap $0.35mm$ is $0.010Webers$.

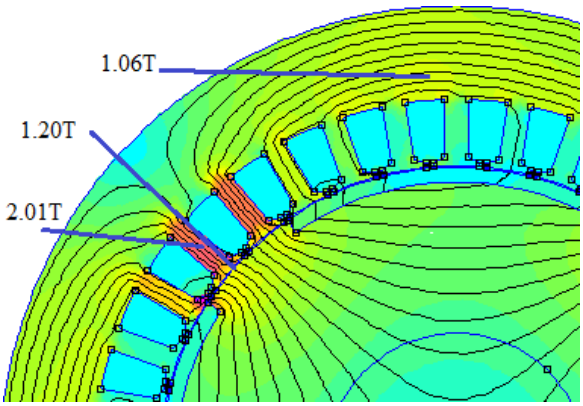

Figure 5-25: Flux density of plot of Inset PMs machine with air gap $0.35mm$

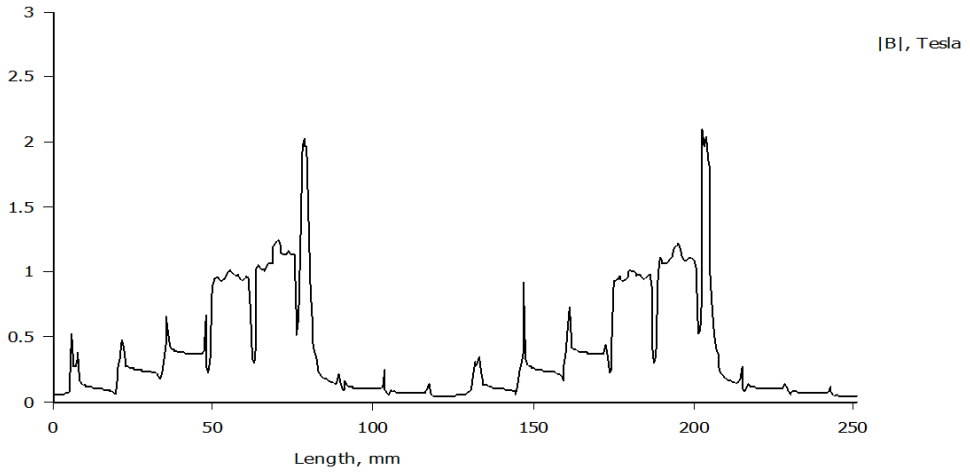

Figure 5-26: Air gap flux density of Inset machine with air gap $0.35mm$

5.4.4 Summary of Optimization

Table 5-2 summarizes the key optimization results of Inset PMs machine. Average torque is increased by 7% but torque ripple is also increased. There is no significant increase in efficiency of machine though air gap is reduced half.

5.5 Analysis of Interior PMs Machine

Different rotor geometry have been tuned and analysed by FEMM since appropriate shape of rotor plays an important role in motor performance. This section investigates the electromechanical characteristics of Interior PMs machine with air gap $0.7mm$. Several simulations were carried out to analyse the model and provided the information about regarding performance characteristics.

Table 5.2: Comparison of Optimized Results with Base Model of Inset PMs Machine

Parameters	Unit	Airgap $0.7mm$	Airgap $0.35mm$
Average Torque	Nm	94.61	101.30
Average Total Loss	Watts	1733.87	1746.81
Ripple	%	82.51	109.91
Efficiency	%	94.49	94.80

5.5.1 Finding MTPA angle of Interior PMs Motor

A simulation was carried out to calculate maximum torque by varying the angle of phase current of Interior PMs motor. It is clearly shown that maximum torque is obtained at current angle of $134degree$ for phase current of $600Amps$ is shown in Figure 5-14. Advance angle of this machine can be calculated as angle between q-axis and position of phase current at MTPA angle and obtained advance angle is $44degree$. So, I_d and I_q currents are calculated at MTPA angle are $-431.60Amps$ and $416.80Amps$, respectively. It should be noted that some negative torques are obtained for some initial phase current angles and this is because of the fact that value of reluctance torque outweighs its magnet alignment torque counterpart. However, these values are discarded when plotting the torque with respect to current angle.

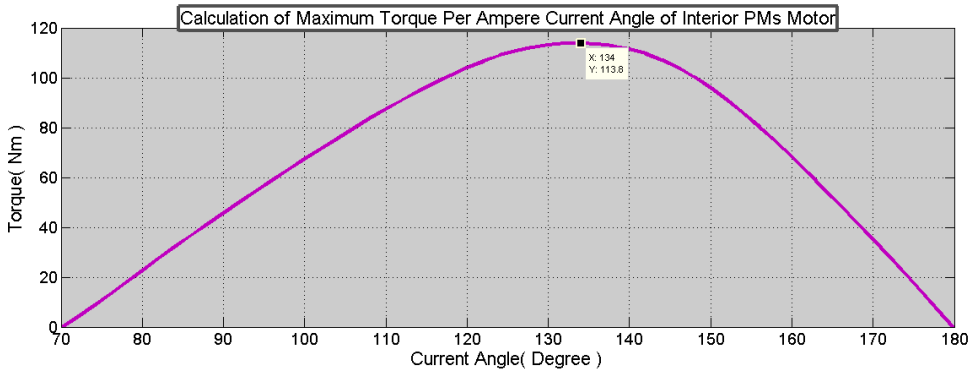

Figure 5-27: Calculation of maximum torque per ampere current angle for Interior PMs machine air gap $0.7mm$

5.5.2 Calculation of Electromechanical Performance of Inset PMs with Air Gap 0.7mm

The instantaneous torque of Interior PMs motor with air gap $0.7mm$ was calculated for equally spaced 45 angular position over one half of the pole pitch and then results were averaged. As can be seen from the graph, magnitude of toque went

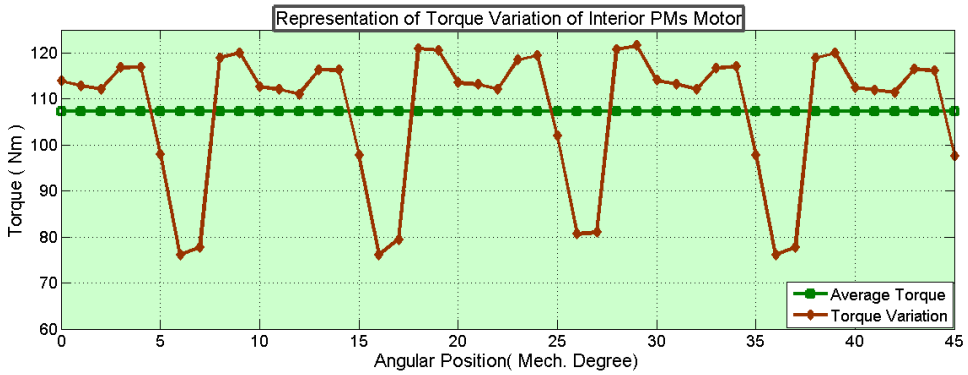

Figure 5-28: Behaviour of torque with respect to Interior PMs machine

up and down widely over the whole angular position of rotor. Value of maximum torque is calculated of $121.56Nm$ at rotor position $29degree$ and minimum torque is calculated as $76.08Nm$ at rotor position 6 degree. Average torque and torque ripple is reported for this topology are $107.33Nm$ and 42.38%

Figure 5-29 depicts the different losses of Interior PMs motor with air gap $0.7mm$. It is worth noting here that Interior PMs machine is the most lossiest machine among all machine studied previously. Iron losses are higher than any other machine which pushes the average losses to $2161.44watts$.

5.5.3 Density Map of Interior PMs Motor with Air Gap 0.7mm

As expected, resultant flux lines are higher in Interior PMs motor is shown in Figure 5-30 because of higher volume of PMs in the rotor. The dimensions of magnet is length =60mm, breadth =5mm, height=220mm. As is shown in Figure 5-30, saturation of flux is observed corresponding to the area of stator teeth and back iron core and measured fluxes are $2.04T$ and $1.61T$, respectively.

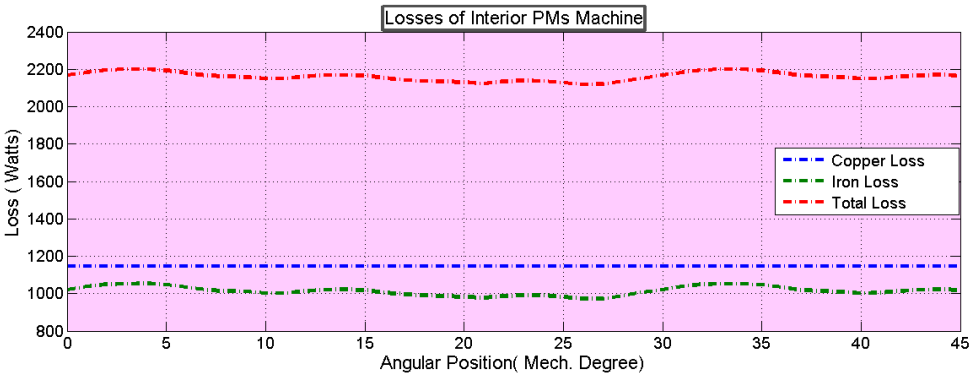

Figure 5-29: Measured different losses of Interior PMs machine with air gap 0.7mm

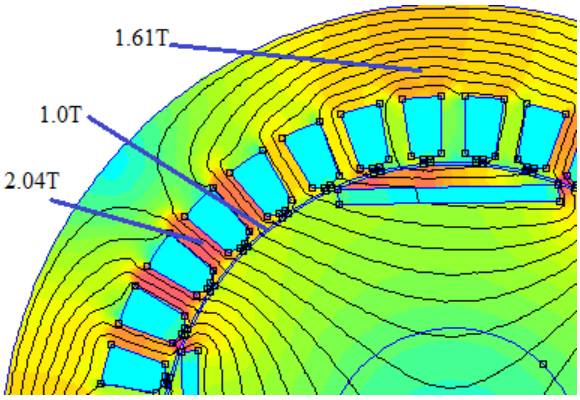

Figure 5-30: Flux density of plot of Interior PMs machine with airgap 0.7mm

Normal component of average flux per pole of Interior PMs motor with airgap $0.7mm$ is estimated of $0.017Webers$. Air gap flux density of Interior PMs has been drawn by means of 2D finite element analysis is shown in Figure 5-31. It is clearly shown that effect of eighteen slots on flux density is prominent since the analysis covers circumference of eighteen slots.

5.5.4 Flux Linkage of Interior PMs Machine with Air-gap 0.7mm

The line graph, as shown in Figure 5-32, illustrates the value of flux linkage along the d-axis and q-axis. At zero current, d-axis flux linkage was higher than q-axis flux linkage due to presence of magnet flux in the d-axis. However, value of q-axis flux linkage has exceeded d-axis flux linkage for applied current of $100Amps$. Difference in values between d- and q-axis has been reduced for the following applied currents.

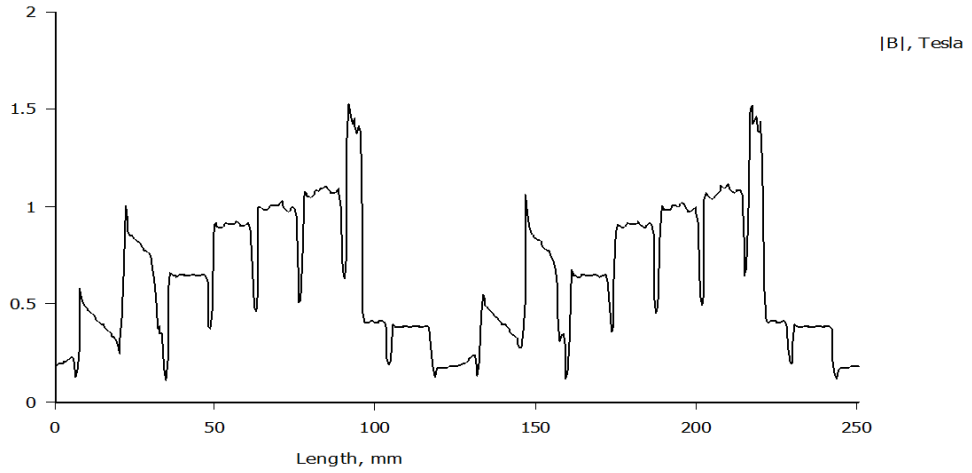

Figure 5-31: Airgap flux density of Interior PMs motor with airgap $0.7mm$

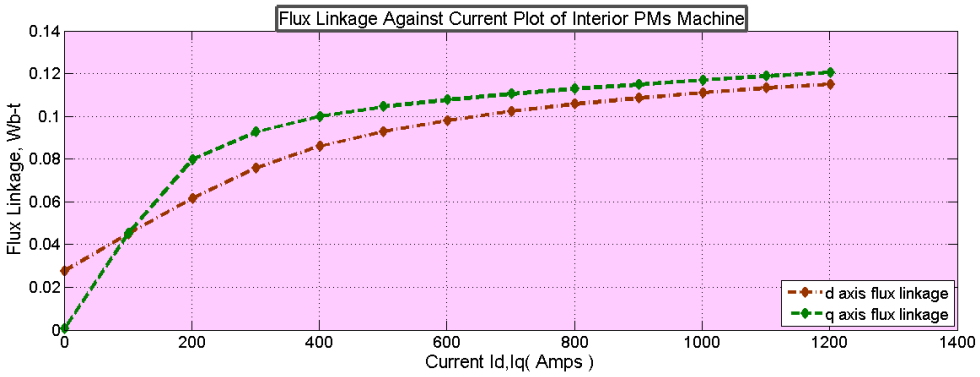

Figure 5-32: Plot of d- and q-axis flux linkages vs. Current in Interior PMs machine

5.5.5 Inductances and Saliency Ratio

Figure 5-33 depicts d- and q-axis inductances of Interior PMs motor with air gap of $0.7mm$. As is illustrated by the graph, there is a huge difference between the value of L_d and L_q for initial some current values. Largest difference in values between L_d and L_q implies that greatest reluctance torque capability. The value of L_q is decreased dramatically for the higher values of currents. Saliency ratio is measured as L_d/L_q and obtained graph is shown in Figure 5-34. Saliency ratio is increased gradually with increasing applied stator current. It is clearly seen that maximum and minimum saliency ratio for entire current range are 0.73 and 0.36, respectively. This implies that at higher current value of L_d and L_q is getting closer.

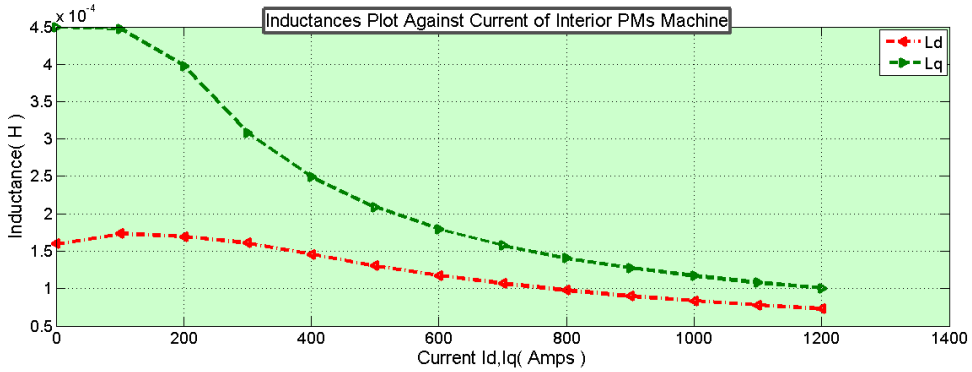

Figure 5-33: Measured inductances as a function of current of Interior PMs machine

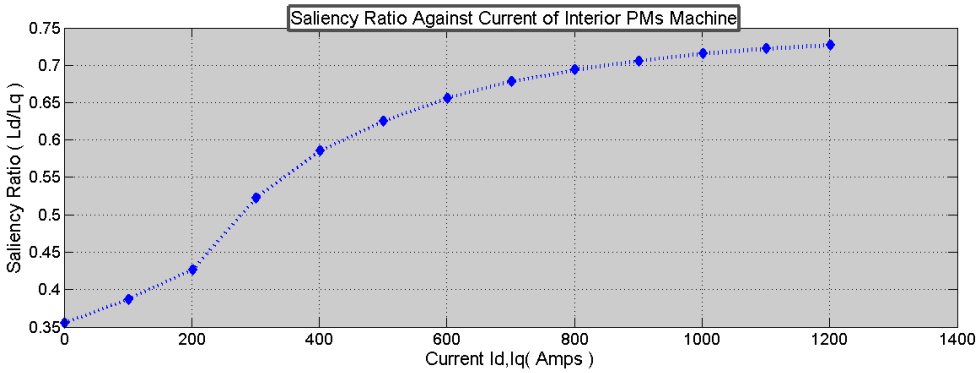

Figure 5-34: Saliency ratio (L_d/L_q) as a function of current of Interior PMs motor with air gap $0.7mm$

5.6 Optimization of Interior PMs motor

A new FEM model with reduced air of 0.35mm has been created with aim to optimize the motor performances. Key machine performances have been explored by means of several similar simulations in FEM environment. Following sections compare and contrast the results of new model with old model of Interior PMs motor.

5.6.1 Comparison of MTPA Angles

Finite element analysis can be used to generate maximum torque for new Interior PMs model by varying the current angle while phase current is set to $600Amps$. Maximum torque has been calculated at phase current angle 132 degree while $I_d = -401.50Amps$ and $I_q = 445.90Amps$. The MTPA current angle has been shifted to left by $2degrees$ of optimized model.

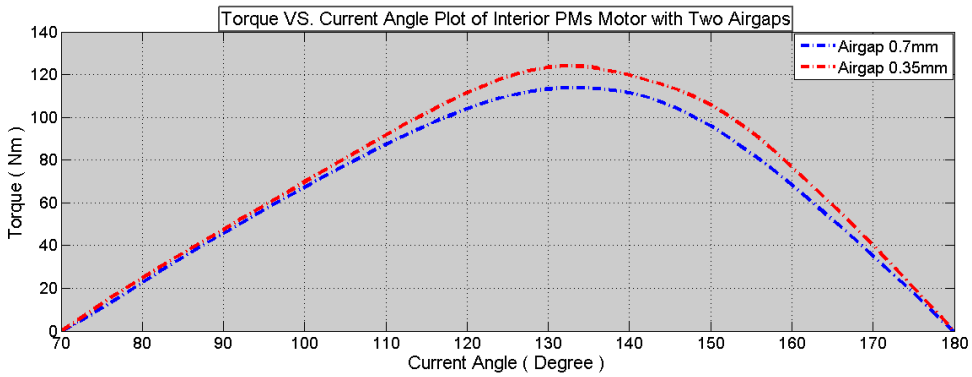

Figure 5-35: Plot of torque vs. Current angle for two different air gaps in Interior PMs machine

5.6.2 Comparison Performance Parameters

A simulation was carried out to calculate torque of optimized model of Interior PMs motor. Torque has been calculated with respect to angular position of rotor, moving the rotor of 45 degree mechanical. Behaviour of the torque of both models are plotted in a same graph is shown in Figure 5-36. One of the interesting results observable in Figure 5-36, gap in maximum and minimum value of torque is widen in optimized model. As can be seen from the graph, maximum value of torque is reported of 144.91Nm where minimum value is only 47.65Nm which yields very high torque ripple of 85.15%. Figure 5-37 depicts efficiency as a function of angular position of

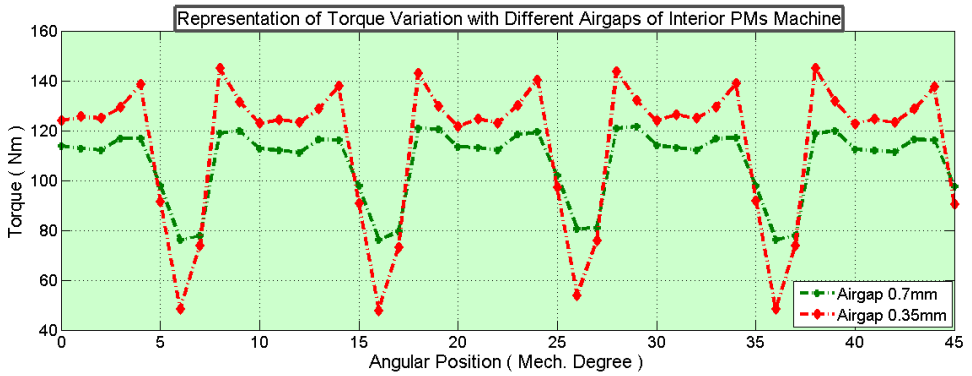

Figure 5-36: Comparison torque variation with respect to current angle for two different air gaps in Inset PMs machine

rotor of Interior PMs machine with air gap 0.35mm. Average efficiency is reported of 93.53% while maximum and minimum efficiency are 95.31% and 86.80%, respectively.

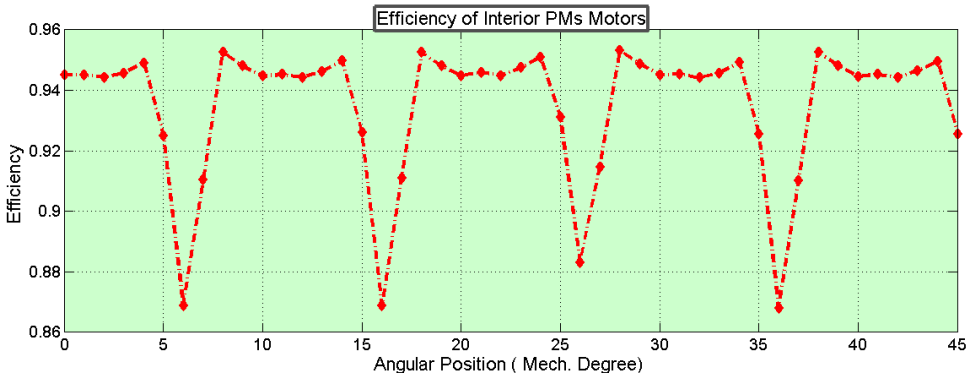

Figure 5-37: Measured efficiency of Interior PMs machine with air gap $0.35mm$

5.6.3 Density Map of Interior PMs Motor with Air Gap 0.35mm

As expected, resultant flux lines is higher in optimized design is shown in Figure 5-38. As can be seen from density map, there has been an increase of flux density in areas corresponding to stator teeth and back iron core and their maximum values are $2.06T$ and $1.73T$, respectively. A contour is covered semicircle through the air

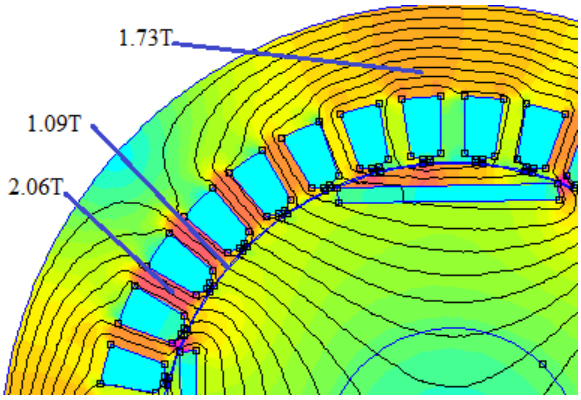

Figure 5-38: Flux density of plot of Interior PMs machine with air gap $0.35mm$

gap has been drawn in order to draw the flux density plot by means of FEM in post processing mode. Air gap flux density of Interior PMs motor is reported in Figure 5-39. Here, slotting effect is more prominent than other machines. It is important to note that normal component of average flux per pole of Interior PMs motor with air gap $0.35mm$ is 0.018 Webers.

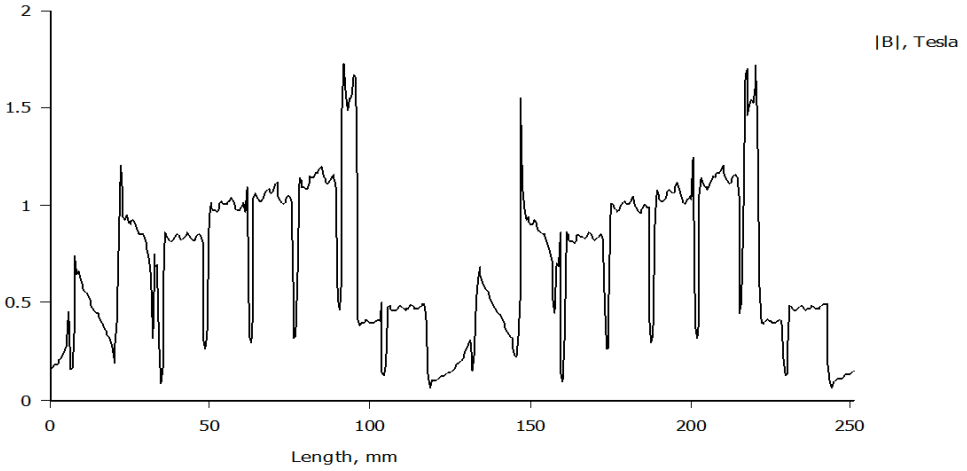

Figure 5-39: Air gap flux density of Interior PMs motor with air gap 0.35mm

Table 5-3 gives information on optimized results of Interior PMs machine in terms of the key electromechanical performance parameters. As per the table, the percentage increase in value of torque is by 6.41%, there was slight increase of efficiency since Losses will effects directly to the efficiency of the machine. On the other hand, torque ripple is increased almost doubled which is detrimental effect on machine performance.

Table 5.3: Comparison of Optimized Results with Base Model of Interior PMs Machine

Parameters	Unit	Airgap 0.7mm	Airgap 0.35mm
Average Torque	Nm	107.33	114.22
Average Total Loss	Watts	2161.44	2275.80
Ripple	%	42.38	85.15
Efficiency	%	93.98	94.03

5.7 Analysis of PMASR Machine

The purpose of this section is to explore electromechanical characteristics of PMASR machine with air gap 0.35mm. Several similar simulations, as explained before, are carried out to analyse the model and provided the information about regarding performance characteristics.

5.7.1 Finding MTPA angle of PMASR Motor

An investigation has used 2D electromagnetic FE analysis to calculate maximum torque of PMASR motor by varying the angle of phase current from 0 to 90$degree$. MTPA angle is achieved at 65$degree$ is shown in Figure 5-40. So, I_d and I_q currents are calculated at MTPA angle are 253.571A and 543.784A, respectively.

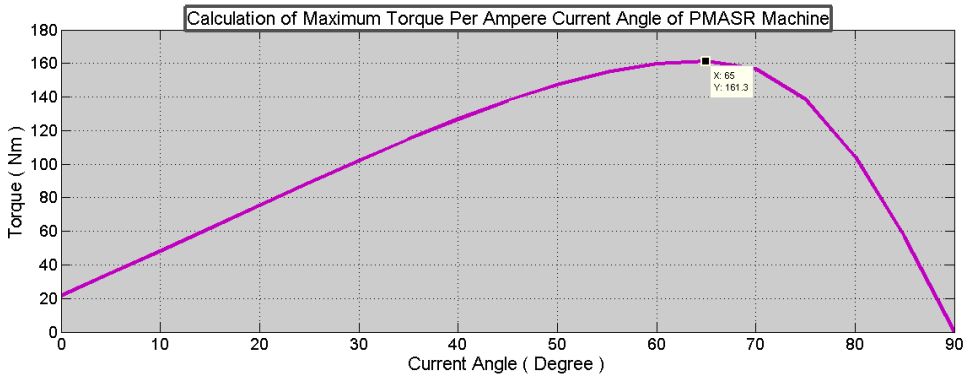

Figure 5-40: Calculation of maximum torque per ampere current angle for PMASR machine

5.7.2 Calculation of Electromechanical Performance of PMASR with Air Gap 0.35mm

Torque of PMASR has been calculated for equally spaced 45 angular positions over one half of the pole pitch. Average output torque has been increased due to additional magneto motive force (MMFs) coming from PMs even for the same stator input currents. Average torque is estimated of 148.60Nm. From the graph it is clear that there is a little gap between minimum and maximum value of torque which yields to minimum torque ripple of 17.48%.

Different losses of PMASR are depicted in Figure 5-42 with respect to angular position of rotor. Copper loss is fixed for all machines, as explained earlier. As can be seen from the graph, total loss of this machine is a bit lower than Interior PMs. Average copper and total losses are estimated of 958.49$Watts$ and 2105.39$Watts$, respectively. The line graph, as shown in Figure 5-43, presents the efficiency of PMASR motor. As is illustrated by the graph, it is the highest efficient machine

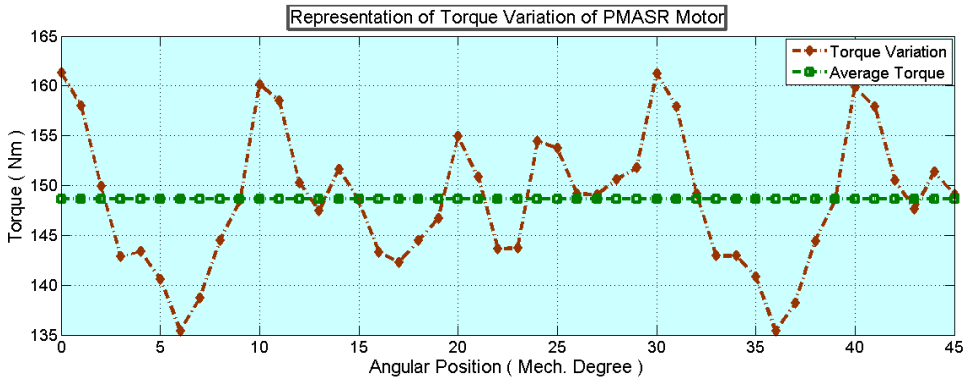

Figure 5-41: Behaviour of torque variation with respect of angular position of PMASR machine

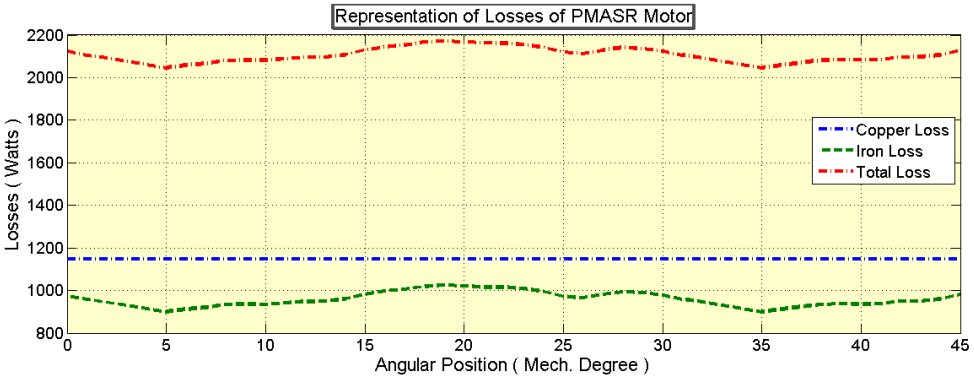

Figure 5-42: Measured different losses of PMASR machine

though loss of this machine is substantially higher than SPM and Inset PMs machine. Average efficiency of PMASR machine is 95.68%.

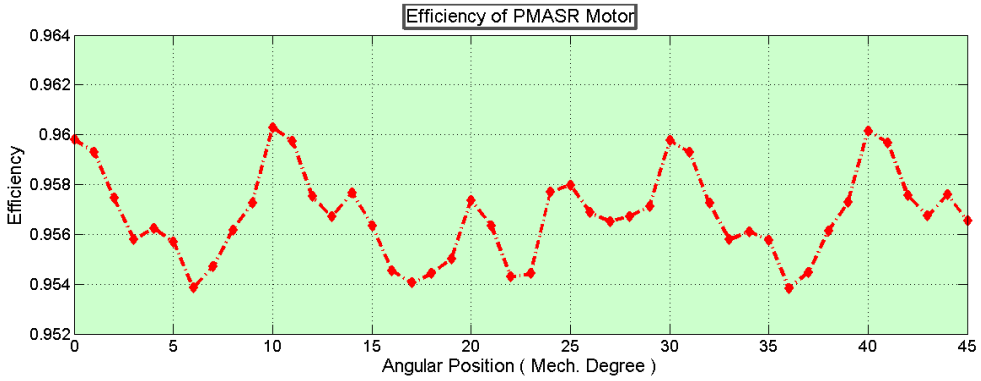

Figure 5-43: Measured efficiency of PMASR machine

5.7.3 Density Map of PMASR Motor with Air Gap 0.35mm

A full load analysis is performed same as previous machines in order to estimate the flux level at full load condition. Flux density map is depicted in Figure 5-44. As is shown by the graph, it shows the local saturation, especially in the areas corresponding to rotor iron ribs and stator teeth as well. Maximum flux density of rotor iron ribs is calculated of $1.45T$. Similarly, Maximum flux in the areas corresponding to stator teeth and back iron core are estimated of $1.93T$ and $1.57T$, respectively. It is impor-

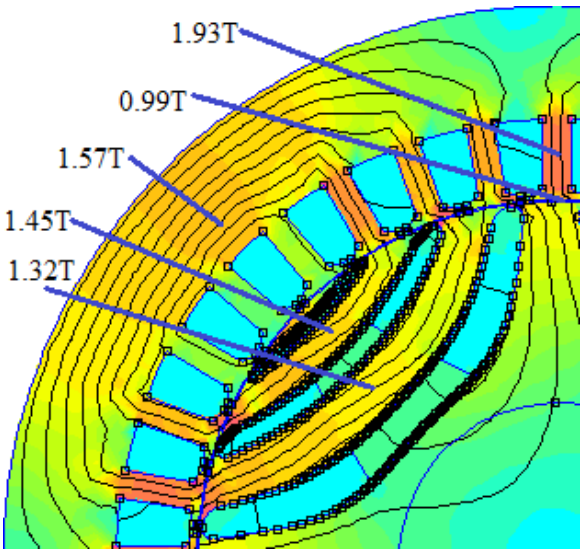

Figure 5-44: Flux density of map of PMASR machine with airgap $0.35mm$

tant to highlight that normal component of average flux per pole of PMASR motor with air gap $0.35mm$ is only $0.0013Webers$. Figure 5-45 discloses air gap flux density of PMASR machine. It should be noted that data was taken for half of circumference of machine. It is shown from Figure 5-45, slotting effect is highly noticeable at slot position.

5.7.4 Flux Linkage of PMASR Machine with Air-gap 0.35mm

Figure 5-46 shows flux linkage along the d- and q-axis of PMASR motor with air gap $0.35mm$. From the graph it is clear that q-axis flux linkage shows linear relationship with whole applied currents. For stator current between $0A$ and $300A$, value of d-axis flux linkage is experienced dramatic increase. From current $300A$ to $1200A$ the value of d-axis flux linkage remained fairly unchanged.

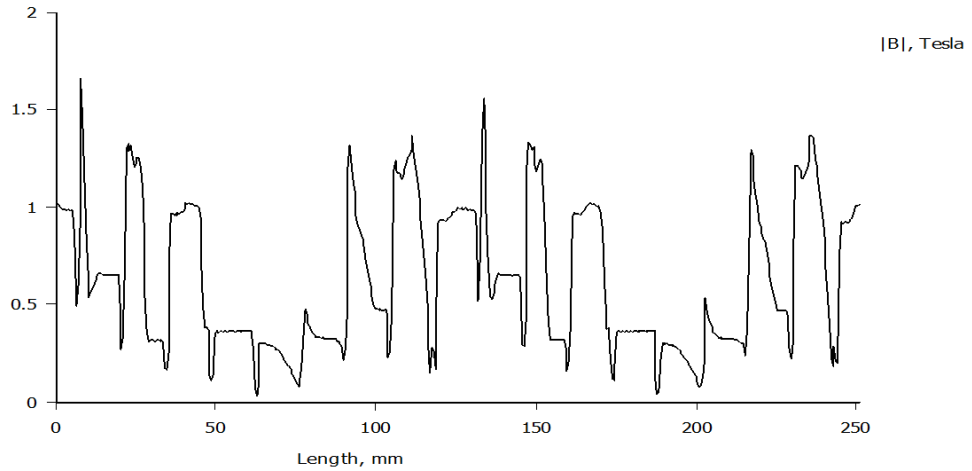

Figure 5-45: Air gap flux density of PMASR motor with air gap $0.35mm$

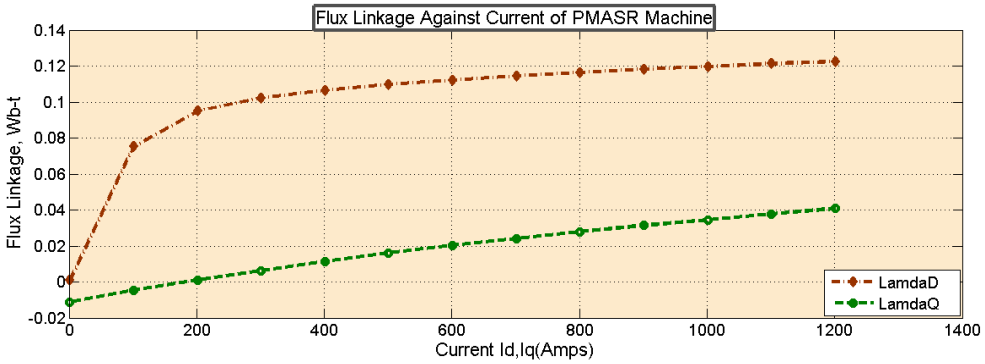

Figure 5-46: Plot of d- and q-axis flux linkages vs. Current in Interior PMs machine

5.7.5 Inductances and Saliency Ratio

It can be seen from Figure 5-47, value of d-axis inductance, L_d, is far greater than q-axis inductance, L_q, for some initial values of currents. As is observed from the graph, gap between L_d and L_q has been reducing greatly for higher currents. There has been a sudden spike at applied current $200Amps$ in the saliency ratio (L_d/L_q) graph as shown in Figure 5-48. After that there is a gradual decrease the value of saliency ratio. Indeed, high saliency ratio helps to give the high reluctance torque in this machine.

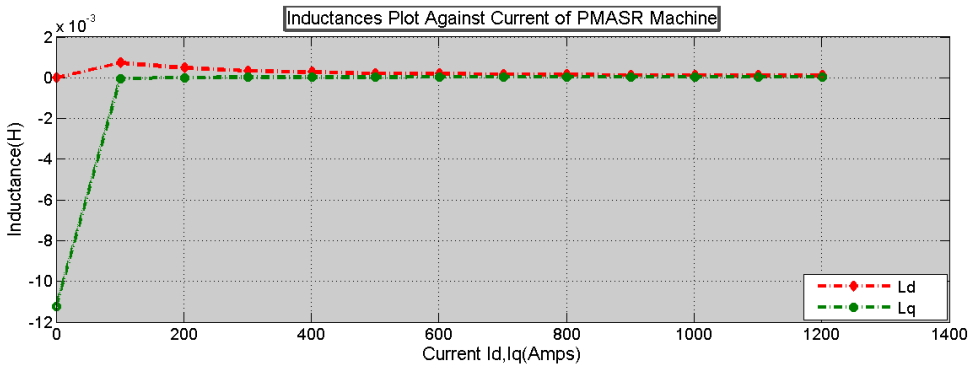

Figure 5-47: Measured inductances as a function of current in PMASR machine

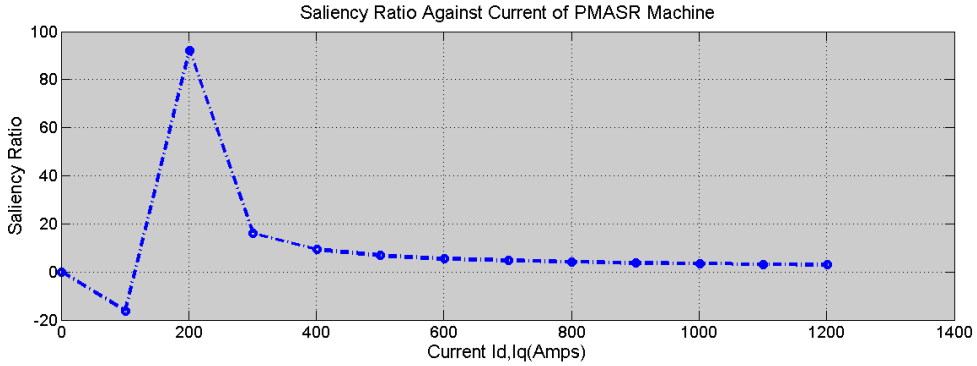

Figure 5-48: Saliency ratio (L_d/L_q) as a function of current in PMASR machine

5.8 Comparison of Four Models

This section deals with comparison and contrast among first four motor topologies, are considered in this analysis. In order to provide a substantive comparison, let us

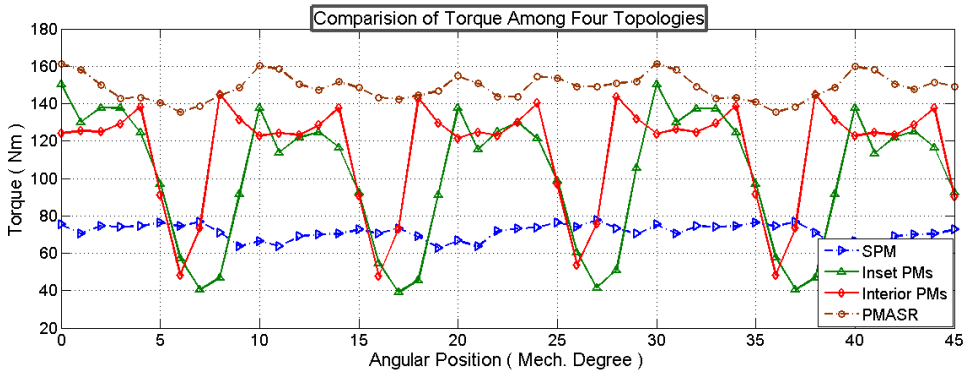

Figure 5-49: Comparison of torque variation with respect to angular position among four different machine with airgap $0.35mm$

consider the Interior PMs machine as reference machine for following comparisons. It

Table 5.4: Comparison of Key Parameters Among Four Models

Parameters	Unit	SMPM	Inset PMs	Interior PMs	PMASR
Average Torque	Nm	71.34	101.30	114.21	148.35
Peak Torque	Nm	77.62	150.46	144.91	161.32
Peak Current	Amps	600	600	600	600
Base Speed	rpm	3000	3000	3000	3000
Average λ_D	Web-t	0.0378	0.0002	0.0086	0.0947
Average λ_Q	Web-t	0.0498	0.0690	0.1037	0.0098
Average L_d	H	7.56^{-5}	8.70×10^{-5}	0.00014	0.0002
Average L_q	H	8.11×10^{-5}	0.000183	0.00029	-0.00084
Total Loss	Watts	1590.16	1746.80	2275.79	2112.80
Average Iron Loss	Watts	443.26	599.90	1128.89	958.48
Ripple	%	20.92	109.90	85.15	17.47
Average Efficiency	%	93.98	94.80	94.03	95.66

is worth noting that key electromechanical performances have been evaluated in the d-q reference frame and for the same air gap of $0.35mm$. Table 5-4 summarizes main key electromechanical results. PMASR has the maximum value of average and peak torque among all topologies. Value of peak current and base speed are same for all machines.Maximum value of d-axis flux linkage is observed in PMASR machine and maximum value of q-axis flux linkage is calculated in Interior PMs machine. Though PMASR is the second highest lossy machine, it is achieved the highest efficiency and this is because of the its highest average torque.

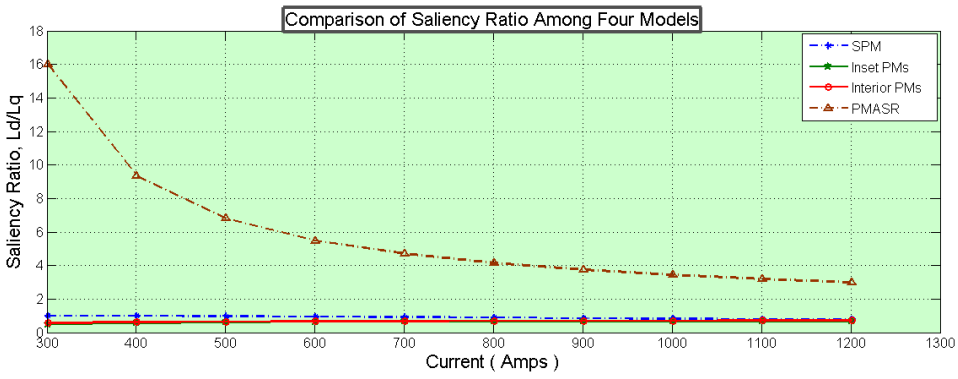

Figure 5-50: Comparison of saliency ratio (L_d/L_q) as a function of current among four different machines with airgap $0.35mm$

Figure 5-49 illustrates torque variation of four topologies. As is observed from graph, Inset PMs machine shows similar trend of Interior PMs machine's torque.

Both machines have high torque ripple and their obtained torque ripples are 109.90% for Inset PMs and 85.15% for Interior PMs machines. On the other hand, SMPM and PMASR follow opposite trends as both are lower torque ripple machines. It is clearly seen that PMASR is the highest and SMPM is the lowest average torque machines among all topologies.

An interesting fact is that among four topologies, three machines such as SMPM, Inset and Interior PMs machine have almost same saliency ratio, and their saliency ratio in between 0-1, as shown in Figure 5-50. In contrast, PMASR is shown to be the highest salient and most preferable machine.

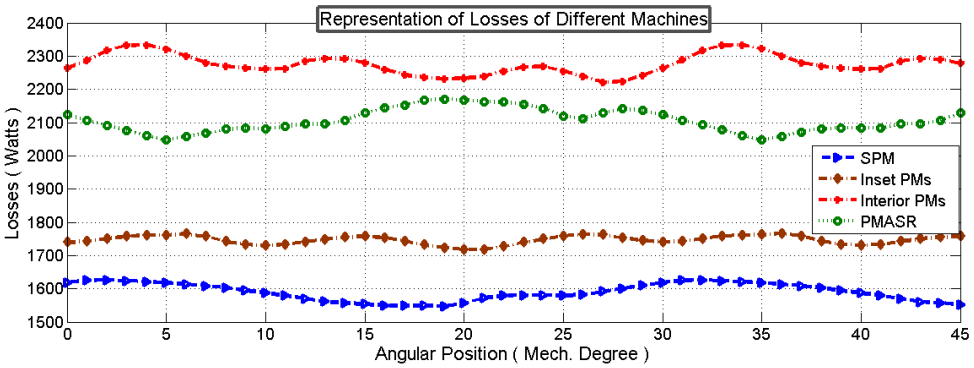

Figure 5-51: Comparison of losses among four different machines with same airgap $0.35mm$

As is observed from Figure 5-51, SMPM machine shows the least value of losses among all topologies. This is quite less in terms of loss of Interior PMs machine. Average loss of PMASR is 7.48% less than Interior PMs machine. Similarly, average loss of Inset PMs machine is 23.24% less than Inset PMs machine. Among all topologies PMASR is the highest efficient machine though it is incurred second highest losses.

Chapter 6

Analysis of FEMM Results of SynR Machines

Synchronous Reluctance (SynR) machine is one type of reluctance machine where torque is determined by magnetic reluctance. SynR does not have PMs in the ferromagnetic rotor. SynR machine have the same number of magnetic poles in the stator and in the rotor. Rotor losses are lower in compared with induction machine. However, it requires the variable- frequency drive in order to control speed.

In this chapter, FEMM results of two different configurations of SynR machine are investigated based on analysis procedures discussed in earlier chapter. This chapter examines the key electromechanical performance parameters of Synchronous Reluctance (SynR) machine and Segmented Synchronous Reluctance (SegR) machine. Last section in this chapter is dealt with comparisons and contrasts on some of the electromechanical parameters of both reluctance machines.

6.1 Analysis of SynR Machine

This section evaluates the performances of SynR machine with air gap $0.35mm$. Several simulations were carried in step by step in order to examine key machine performances parameters.

6.1.1 Finding MTPA angle of SynR Motor

Like in PMASR, almost similar simulation was carried out to estimate the maximum torque of PMASR machine. It should be noted that data was taken for every $5degrees$ increment up to $90degrees$ of phase current angle. Figure 6-1 shows the MTPA angle calculation of SynR machine with air gap of $0.35mm$. It can be seen from the graph, the maximum torque of $151.99Nm$ is achieved at current angle $65degree$. I_d and I_q currents are recorded at MTPA angle $253.57Amps$ and $543.78Amps$.

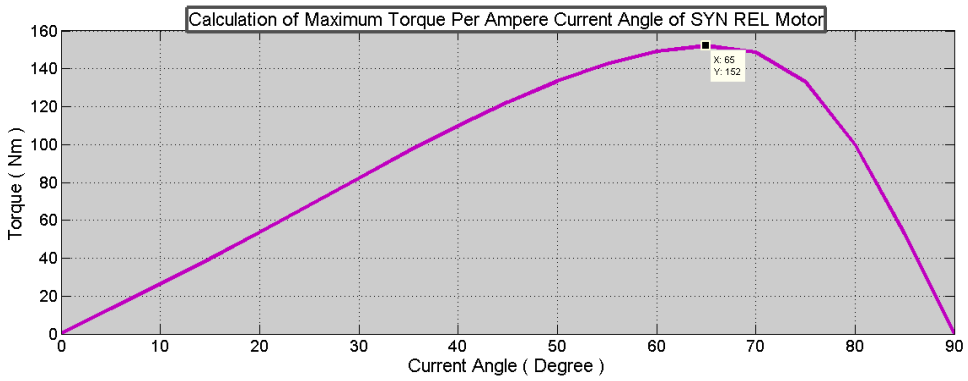

Figure 6-1: Calculation of maximum torque per ampere current angle for Synchronous Reluctance machine

6.1.2 Calculation of Electromechanical Performance of SynR with Air Gap 0.35mm

Figure 6-2 illustrates the instantaneous value of torque of SynR machine with air gap of $0.35mm$. As is observed from the graph, the value of torque went up and down from the average value for the entire $45degree$ mechanical rotation of rotor. Average torque is calculated of $137.55Nm$ where value of maximum and minimum torque are $152.10Nm$ and $121.55Nm$, respectively.

It is well known that torque ripple is the main drawbacks for SynR machine but here torque ripple is reported only 22.21%.Iron loss of SynR machine with the air gap of $0.35mm$ remains almost steady state throughout the mechanical rotation of $45degree$. Average of Iron loss is estimated of $993.52Watts$, as shown in Figure 6-3, and corresponding total average loss is reported of $2140.43Watts$.

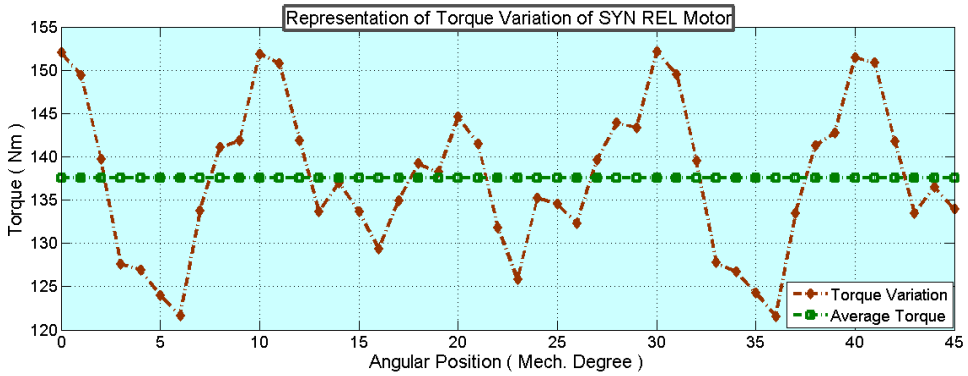

Figure 6-2: Behaviour of torque variation with respect of angular position of Synchronous Reluctance machine

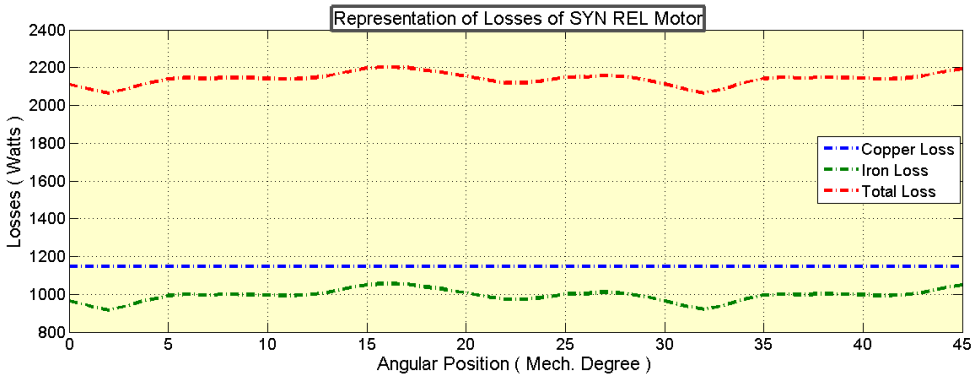

Figure 6-3: Measured different losses of Synchronous Reluctance machine

Figure 6-4 depicts how efficiency of SynR machine varies with angular position of rotor. Maximum and minimum efficiency are found 95.76% at angular position of $30degree$ and 94.67% at angular position of $36degree$, respectively. Average efficiency of this machine is calculated of 95.26% which is pretty good in comparison with other topologies.

6.1.3 Air Gap Flux Density Plot of SynR Machine with Air Gap 0.35mm

It is clearly seen from the Figure 6-5, there is a significant effect on the magnetic field distribution of SynR machine with air gap of $0.35mm$. It is to be noted that air gap density plot covers two pole spans which implies it covers half circumference of machine. Normal component of average flux per pole of SYN REL motor with air gap $0.35mm$ is calculated of $0.0036Weber$.

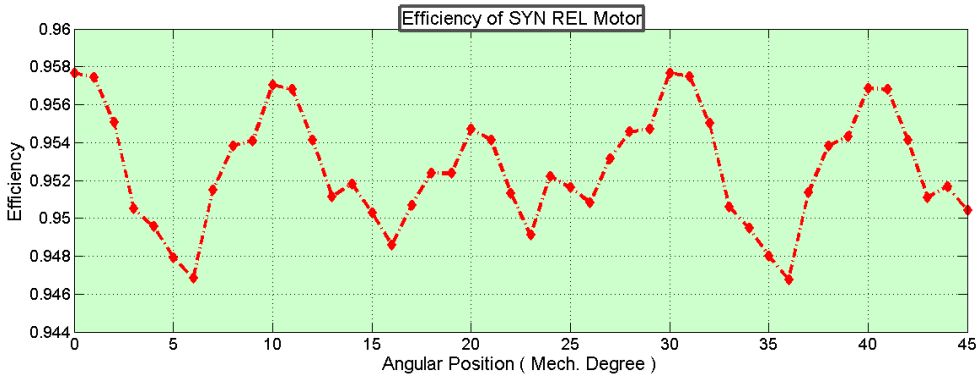

Figure 6-4: Measured efficiency of SYN REL machine

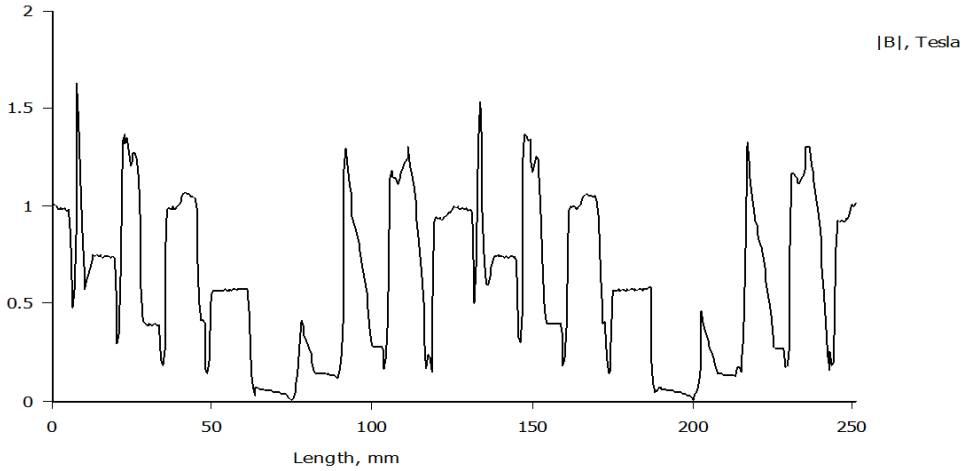

Figure 6-5: Air gap flux density of SYN REL motor with air gap $0.35mm$

6.1.4 Flux Linkage of SynR Machine with Air-gap 0.35mm

Characteristics of flux linkage along d and q-axis of SynR machine is shown in Figure 6-6. As can be seen from the graph, q-axis flux linkage shows linear relationship with I_q current. But saturation is observed in d-axis flux linkage graph at applied I_d current of $300Amps$. There is a significant increase in the value of d-axis flux linkage between I_d current of $0Amps$ and $300Amps$.

6.1.5 Inductances and Saliency Ratio of SynR Machine

The larger the difference between the value of L_d and L_q the more capability of getting reluctance torque. There is a significant difference in values between d- and q-axis inductances in SynR machine with air gap of $0.35mm$, as shown in Figure 6-7. This characteristic facilitates the getting larger reluctance torque. Figure 6-8

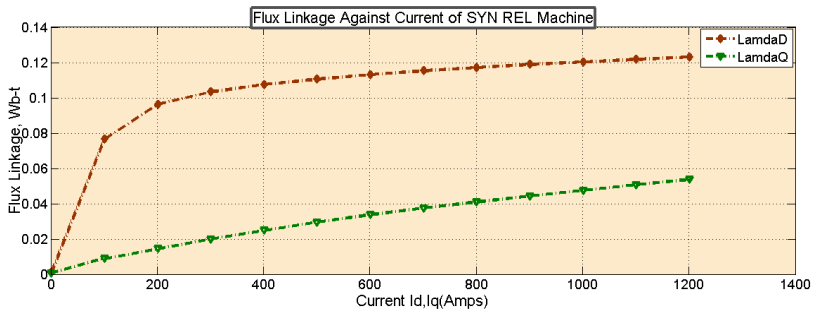

Figure 6-6: Plot of d- and q-axis flux linkages vs. Current of SYN REL machine

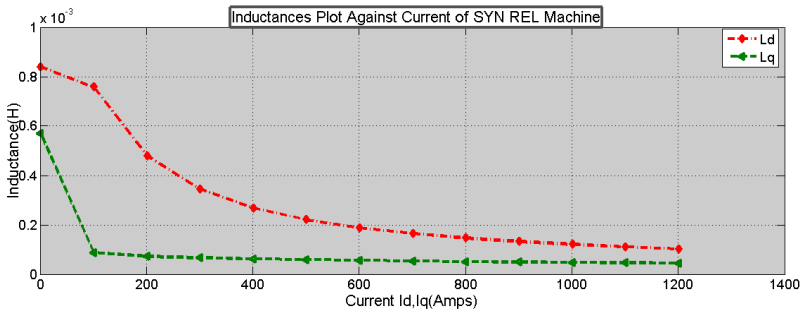

Figure 6-7: Measured inductances as a function of current SYN REL machine

shows the saliency ratio of SynR machine with air gap of $0.35mm$. Maximum saliency ratio is reported of 8.6 and saliency ratio has been reduced to 2.2 at applied current $1200Amps$.

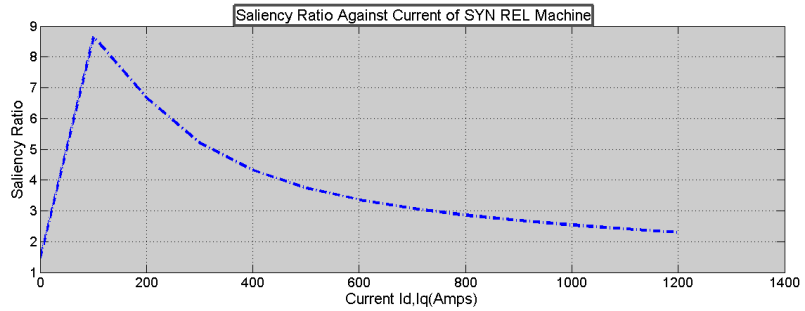

Figure 6-8: Saliency ratio (L_d/L_q) as a function of current of SYN REL machine

6.2 Analysis of Segmented REL Machine

The aim of this section is to evaluate the FEMM model of SEG REL machine with air gap $0.35mm$ and to provide the information about electromechanical performances. Similar simulations were used to determine machine characteristics.

6.2.1 Finding MTPA Angle of SEG REL Motor

A simulation was designed in order to investigate the MTPA angle of SEG REL machine. A simulation is employed for every 5 degree increment up to 90 degree of phase current angle. Figure 6-9 shows the MTPA angle of SEG REL machine with air gap of $0.35mm$. As is illustrated by the graph, maximum torque of $106.29Nm$ is achieved at angle of $65degree$, where the value of I_d and I_q are $253.57Amps$ and $543.78Amps$, respectively.

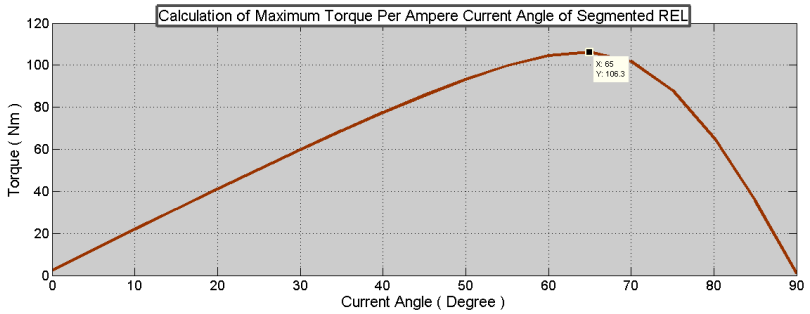

Figure 6-9: Calculation of maximum torque per ampere current angle for Segmented Reluctance machine

6.2.2 Calculation of Electromechanical Performance of SEG REL with Air Gap 0.35mm

Torque variation Figure 6-10 depicts the variation of the torque of SEG REL machine with air gap $0.35mm$. Average value of torque over one half of the pole pitch is reported of $96.13Nm$. Maximum torque is calculated of $124.77Nm$ at angular

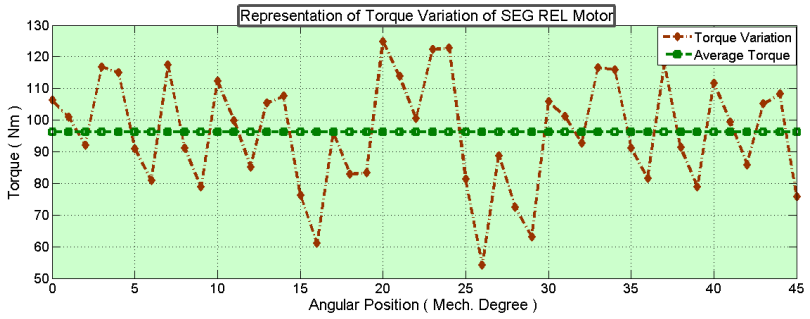

Figure 6-10: Behaviour of torque variation with respect of angular position of Synchronous Reluctance machine

position of rotor 20 degree where minimum torque is $54.20Nm$ at angular position of rotor $26degree$. So, electromagnetic torque ripple has been calculated with comparing the average torque and torque ripple is estimated of 73.40%.

Figure 6-11 shows the results of various losses of SEG REL machine with air gap of $0.35mm$. It can be seen from the graph, this machine is incurred less Iron loss this is because of the fact that it has less volume of iron. Average full load iron loss of this machine is reported of $495.72Watts$ over the $45degree$ mechanical rotation of rotor and average total loss is $1642.62Watts$. Efficiency of SEG REL machine has been

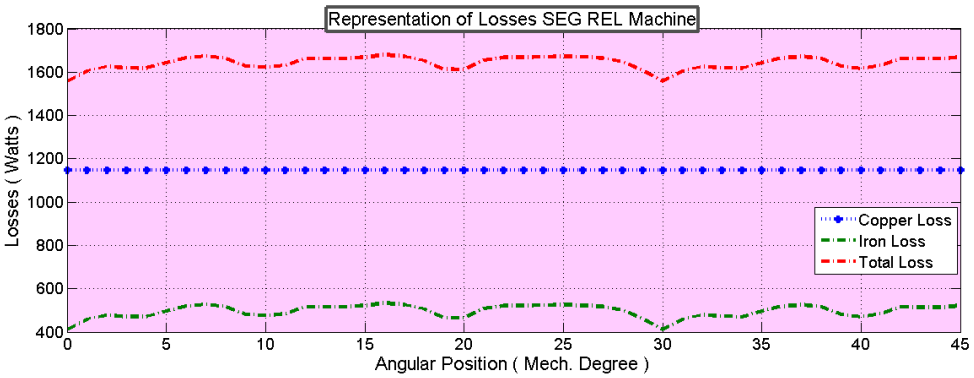

Figure 6-11: Measured different losses of Segmented Reluctance machine

evaluated with respect angular position of the rotor. Average efficiency is calculated 94.66% over $45degree$ mechanical rotation of rotor where maximum and minimum efficiency are 96.04% and 91.07%, respectively.

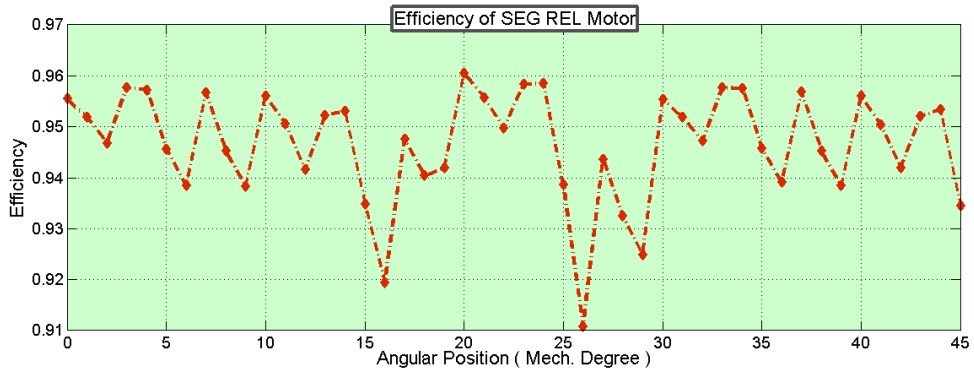

Figure 6-12: Measured efficiency of Segmented REL machine

6.2.3 Air Gap Flux Density Plot of SEG REL Machine with Air Gap 0.35mm

A contour has been drawn through the air gap of SEG REL machine in order to plot the behaviour of air gap magnetic flux distribution. As is observed from Figure 5-13, there is a clear distortion of magnetic flux distribution at position of every stator slots. It should be noted that Normal component of average flux per pole of SEG REL motor with air gap $0.35mm$ is $0.00119119Webers$.

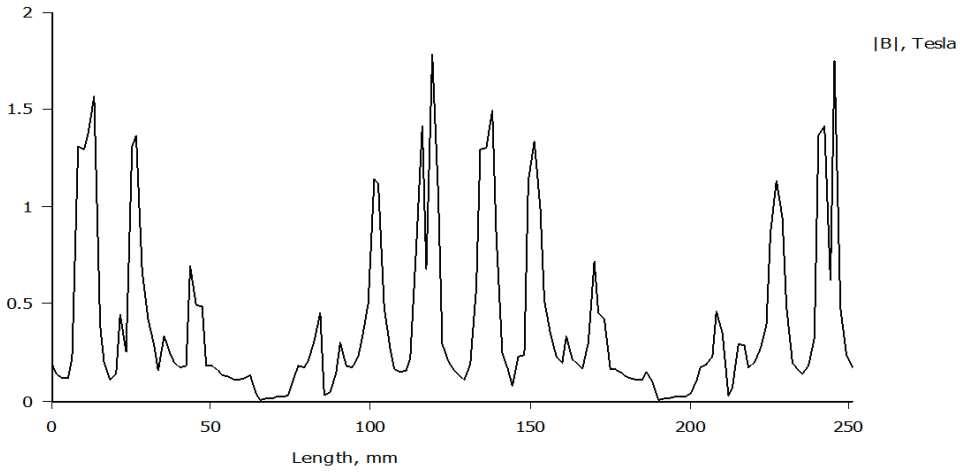

Figure 6-13: Air gap density plot of SEG REL machine with air gap of $0.35mm$

6.2.4 Flux Linkage of SEG REL Machine with Air-gap 0.35mm

Figure 6-14 represents flux linkages along the d- and q-axis versus current for d- and q-axis showing little bit saturation in the d-axis. It is clearly seen that q-axis flux linkage shows linear relationship with I_q current. Similarly, d-axis flux linkage shows also linearity before reaching saturation at applied current I_d of $400Amps$.

6.2.5 Inductances and Saliency Ratio of SEG REL Machine

There is a big difference in values between the d- and q-axis inductances of SEG REL machine with air gap $0.3mm$, as shown in Figure 6-15. This is a biggest difference observed among all machines studied in this thesis. It can be seen from the graph, value of L_q remains almost unchanged even if current I_q is increasing to $1200Amps$. On the other hand, value of L_d has been reduced significantly with increasing I_d

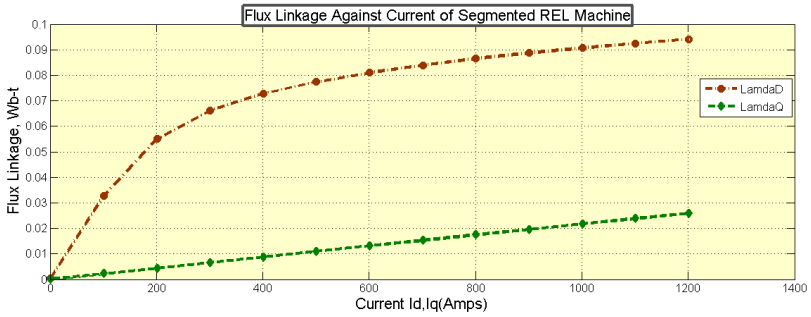

Figure 6-14: Plot of d- and q-axis flux linkages vs. Current of Segmented REL machine

current. Big difference between the d- and q-axis inductances values of SEG REL

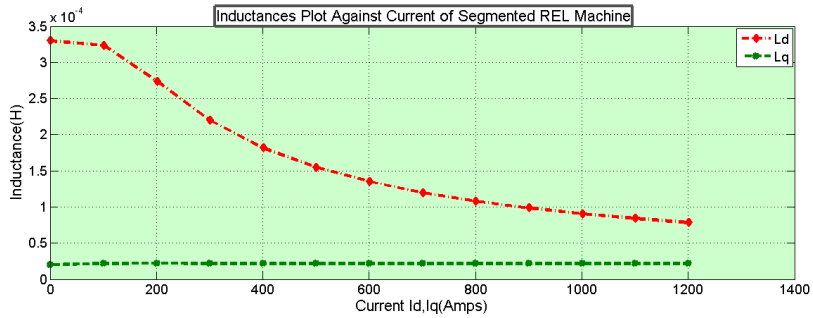

Figure 6-15: Measured inductances as a function of current Segmented REL machine

machine yields to higher saliency ratio. Figure 6-16 shows calculated saliency ratio of SEG REL machine with the air gap of $0.35mm$. There is a gradual decrease in value of saliency ratio with the increasing stator I_d and L_q currents.

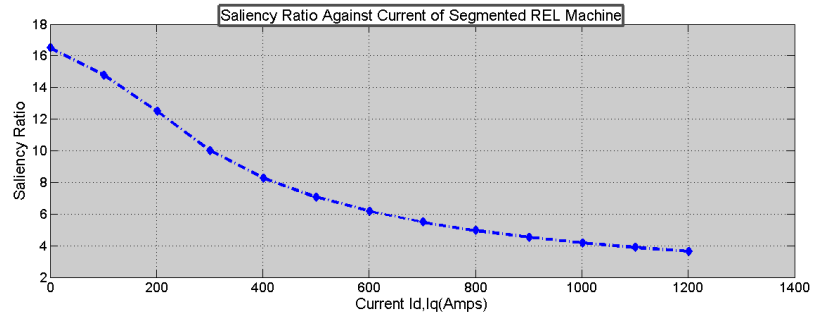

Figure 6-16: Saliency ratio (L_d/L_q) as a function of current of Segmented REL machine

6.3 Comparison Between SynREL and Segmented REL Machines

This section serves as a powerful comparative study between SynR and SEG REL machine. SynR machine has been considered a as reference machine in order to compare with each other holistically. It should be noted that key electromechanical performances data have been evaluated in the d-q reference frame and for the same air gap of $0.35mm$ in both machine. Table 6-1 summarizes main key electromechanical

Table 6.1: Comparison of Results Between SynR and SEG REL Machines

Parameters	Unit	SynREL	SEG REL
Average Torque	Nm	137.55	96.13
Peak Torque	Nm	152.10	124.77
Peak Current	Amps	600	600
Base Speed	rpm	3000	3000
Average λ_D	Web-t	0.094	0.062
Average λ_Q	Web-t	0.023	0.011
Average L_d	H	0.00029	0.00016
Average L_q	H	9.72×10^{-5}	2.17×10^{-5}
Total Loss	Watts	2140.43	1642.62
Average Iron Loss	Watts	993.52	495.72
Ripple	%	22.20	73.40
Average Efficiency	%	95.26	94.66

results which include such as average torque, peak torque, peak current, base speed, average d-axis flux linkage, q-axis flux linkage, d-axis inductance, q-axis inductance,

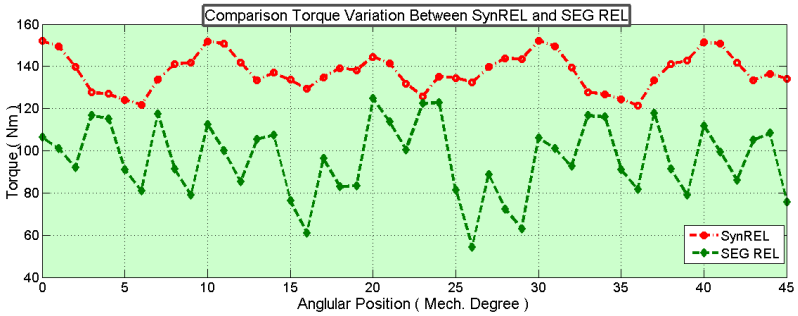

Figure 6-17: Comparison of torque variation with respect to angular position between Synchronous REL and Segmented REL

average total loss, average iron loss, ripple and average efficiency.

Value of average and peak torque of SynREL machine are higher than SEG REL machines values. Similarly, d-and q-axis flux linkage of SynREL machine are evaluated greater value than corresponding values of SEG REL machine. Value of average iron loss of SEG REL machine is almost half the total average value of SynREL machine. Figure 6-17 shows how the torque curves both machines vary with varying

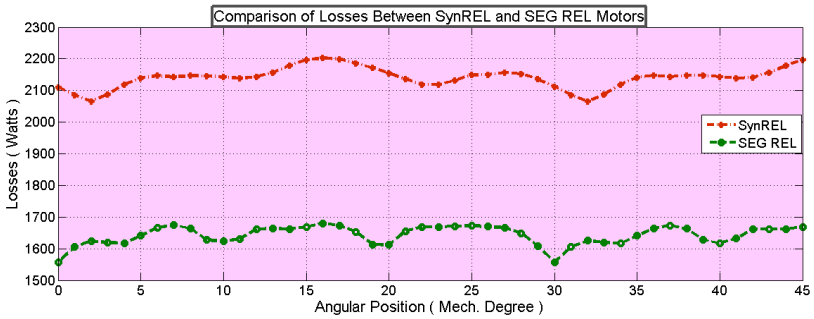

Figure 6-18: Comparison of losses with respect to angular position between Synchronous REL and Segmented REL

angular position of rotor. From the graph it is clear that value of torque ripple of SEG REL have more than tripped the value of its counterparts. Value of average full load torque of SEG REL machine is less than 30.11% average torque of SynR according to the information provided in the Table 6-1.

Figure 6-18 shows the estimation of total losses which include iron loss (hysteresis

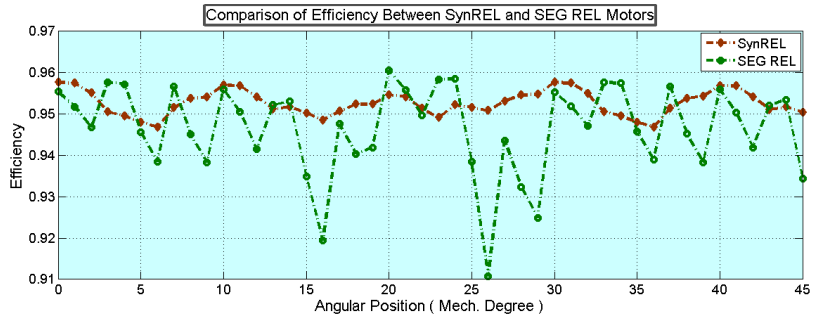

Figure 6-19: Comparison of efficiency with respect to angular position between Synchronous REL and Segmented REL

loss and eddy current loss) and copper loss as well. It can be seen from the graph, calculated value of total loss of SynR machine is far greater than SEG REL machine

total losses. Efficiency of SEG REL went up and down widely over the mechanical rotation of rotor to $45 degree$. Figure 6-19 depicts behaviour the efficiency of both reluctance machines

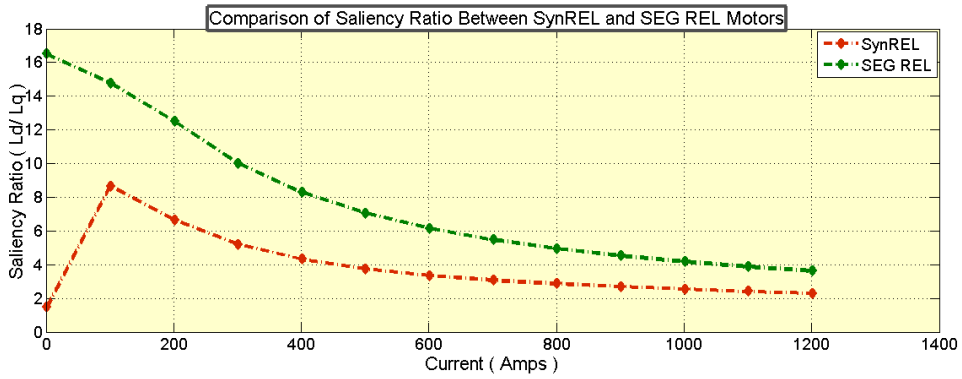

Figure 6-20: Comparison of saliency ratio (L_d/L_q) as a function of current between Synchronous REL and Segmented REL machine.

As is illustrated by the graph, maximum and minimum efficiency of SEG REL is reported of 96.04% and 91.07%, respectively. On the other hand, efficiency of SynR machine remains fairly stable for the entire rotation. Figure 6-20 shows how the

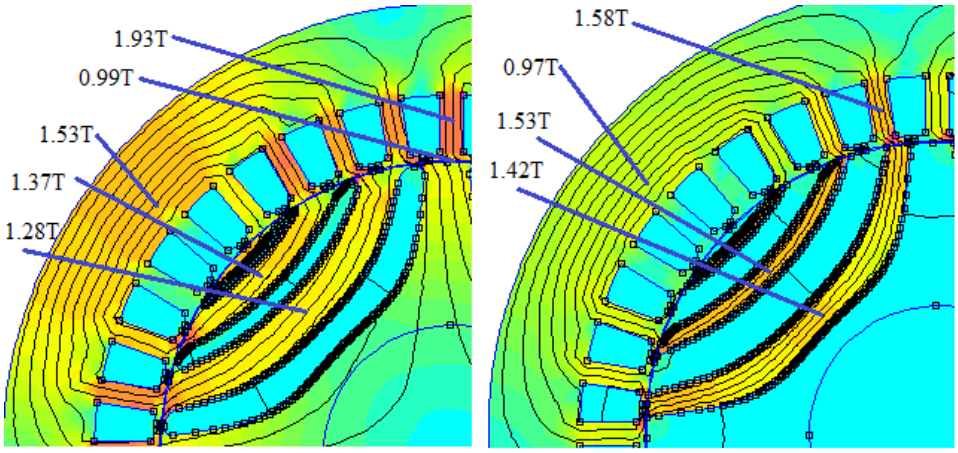

Figure 6-21: Flux density of plot of (a) SYN REL machine and (b) SEG REL machine with airgap $0.35 mm$

saliency ratio of SynREL and SEG REL depends on the ratio of L_d/L_q. From the graph it is clear that value of calculated saliency ratio of SEG REL machine is always greater than the value of saliency ratio of SynR. The L_d/L_q values for SynR machine

are in the range from 1.47 to 8.65 where saliency ratio of SEG REL is in range from 3.63 to 16.5.

A full load analysis is performed in order to estimate the flux density level by analysing density map is shown in Fig. 6-20 (a) SYN REL machine and (b) SEG REL machine with airgap $0.35mm$.

As can be seen from the graph, comparatively lower saturation has been observed in both machines, this is because of absence of PMs in the rotor structure. Flux density level in SynR machine corresponding to the areas to stator teeth and back iron core are higher than the corresponding to the area to SEG REL machine. Flux density of stator teeth of SynR and SEG REL machines are $1.93T$ and $1.58T$, respectively.

Chapter 7

Conclusion and Future Work

Six topologies have been compared and analysed on the basis of same stator geometry and the same number of poles and their relative advantages are studied at particular operating condition. MTPA angle of all machine topologies are found at different current angle.

Analytical model for SMPM machine is deduced and compared with FEMM results in the chapter 4. A sensitivity analysis of SMPM, Inset and Interior PMs is done by changing the air gap and the performance of these machines are studied in detailed using finite element analysis in following chapter 5.

It is shown that optimized models of SMPM, Inset PMs and Interior PMs machines are seen to increase significantly their torque density and efficiency in comparison with their base model.

7.1 Summery of Key Results

The key findings from this thesis are summarized in the following paragraphs.

SMPM machine is not considered to be an ideal option to use in field weakening region though it is low torque ripple machine. This thesis confirms that torque density of Inset and Interior PMs machine is higher than SPM machine. However, they also have substantial torque ripple.

It is always desirable to get ripple results to be minimal at every working condition that can be achieved by minimal variation in the rotor geometry. The problem of high

torque ripple is of course detrimental in the application of precise speed applications.

Efficiency of Inset and Interior PMs machine is affected significantly for the high speed application especially in traction load. This is because of high electrical frequency which incurs high iron losses.

SynR and SEG REL machine show low flux density in the back iron and have possessed low torque density. Moreover, SEG REL machine have demonstrated high torque ripple.

The major disadvantage of IPM machine is often cited to be unexpected inverter shut-down of IPM machine. Uncontrolled flux linkages produced by PMs in IPM machine causes large d-axis current at high speed in the flux weakening region. PMASR is an ideal candidate among all machine topologies because magnet flux linkage in PMASR are in small in comparison with IPM machine. In addition, most of the electromagnetic torque developed in PMASR machine is coming from reluctance torque.

Adoption of ferrite in PMASR design helps to increase power factor and torque capabilities in the PMASR machine with respect to typical SynR machine.

This thesis has demonstrated that the feasibility of PMASR machine in the application variable speed drive is an excellent solution.

It is very strenuous task to deal with coordination among cost, performance and size of machine at the beginning of designing process. So, trade-off among variables is required in order to optimize performance of machine at different situation. The optimal choice between one or other configurations is related to the requested performance.

7.2 Future Research

The followings are the future works that still have to be carried out.

The study of electromagnetic characteristics of six different machine topologies is based on angular position of rotor using finite element analysis. Current simulation is not capable of solving characteristics parameters with respect to rotational speed of rotor. Future work regarding FEM modelling of studied topologies may consider developing a more general analysis in order to get a simulation model which will

include speed of the rotor to evaluate performance parameters.

Further research pertaining to modelling of iron loss in SMPM machine should include effect of flux passing through the rotor cavities while calculating the rotor eddy current losses.

Stray losses model should be included in the simulation as it has deep impact at the time of field weakening operation.

Bibliography

[1] N. Bianchi, S. Bolognani, J. H. Jang, and S. K. Sul. Advantages of inset pm machines for zero-speed sensorless position detection. *IEEE Transactions on Industry Applications*, 44(4):1190–1198, July 2008.

[2] N. Bianchi, M. Degano, and E. Fornasiero. Sensitivity analysis of torque ripple reduction of synchronous reluctance and interior pm motors. *IEEE Transactions on Industry Applications*, 51(1):187–195, Jan 2015.

[3] S. T. Boroujeni and H. B. Naghneh. Analytical modelling and prototyping a slotless surface-inset pm machine. *IET Electric Power Applications*, 11(3):312–322, 2017.

[4] E. Carraro, M. Degano, M. Morandin, and N. Bianchi. Pm synchronous machine comparison for light electric vehicles. In *2014 IEEE International Electric Vehicle Conference (IEVC)*, pages 1–8, Dec 2014.

[5] A. T. de Almeida, F. J. T. E. Ferreira, and G. Baoming. Beyond induction motors 2014;technology trends to move up efficiency. *IEEE Transactions on Industry Applications*, 50(3):2103–2114, May 2014.

[6] A. Fratta, G. P. Troglia, A. Vagati, and F. Villata. Evaluation of torque ripple in high performance synchronous reluctance machines. In *Conference Record of the 1993 IEEE Industry Applications Conference Twenty-Eighth IAS Annual Meeting*, pages 163–170 vol.1, Oct 1993.

[7] L. Guo and L. Parsa. Effects of magnet shape on torque characteristics of interior permanent magnet machines. In *2009 IEEE Electric Ship Technologies Symposium*, pages 93–97, April 2009.

[8] L. Guo and L. Parsa. Torque ripple reduction of the modular interior permanent magnet machines using optimum current profiling technique. In *2009 IEEE International Electric Machines and Drives Conference*, pages 1094–1099, May 2009.

[9] W. L. Soong, P. B. Reddy, A. M. El-Refaie, T. M. Jahns, and N. Ertugrul. Surface pm machine parameter selection for wide field-weakening applications. In *2007 IEEE Industry Applications Annual Meeting*, pages 882–889, Sept 2007.

[10] C. Stancu, S. Hiti, and F. Biais. Maximum torque-per-ampere control of a saturated surface-mounted permanent magnet motor. In *2002 IEEE 33rd Annual IEEE Power Electronics Specialists Conference. Proceedings (Cat. No.02CH37289)*, volume 4, pages 1667–1672, 2002.

Appendix A

Glossary of Symbols and Acronyms

Symbols

V_ϕ = Applied phase voltage

E_A = Back e.m.f. in phase A

X_s = Synchronous reactacnce

I_A = Current in phase A

R_A = Resistance in phase A

λ_A = Flux linkage of phase A

Ψ_m = Magnet Flux

I_d = d- axis current

I_q = q- axis current

ω_r = rotating speed of d-q reference frame

Ψ_d = d-axis flux linkage

Ψ_q = q-axis flux linkage

L_d = d-axis flux inductance

L_q = q-axis flux inductance

L_{md} = d-axis magnetizing inductance

L_{ld} = d- axis leakage inductance

L_{lq} = q- axis leakage inductance

p = Pole pairs

γ_{maxT} = Maximum torque point

ρ_{cu} = Copper resistivity

L_{stk} = Stack lengths

L_{ew} = Lengths of copper conductor

S_{cu} = Cross-section of copper conductor

P_{spec_fe} = Iron losses coefficient

B_{max} = Maximum flux in the considered region

B_{fe_ref} = Reference iron flux density for iron losses calculation

f_{elect} = Electrical frequency for the base speed

f_{ref} = Reference frequency for iron loss calculation

k_{hy} = Specific coefficient of hysteresis loss

k_{ed} = Specific coefficient of eddy current loss

n_c = Number of conductor in one slot

k_{fill} = Slot fill factor

S_{slot} = Slot area

B_{rem} = Remnant magnetic flux density

μ_r = Relative permeability of magnet

k_w = Winding factor

D_e = External diameter

D_s = Inner diameter at the air gap

Q_s = Slot number

h_s = Slot height

w_t = Tooth width

h_{so} = Slot opening width

h_{wed} = Wedge height

h_{bi} = Back iron height

D_{slot} = Slot diameter

g = Airgap

D_{re} = Rotor external diameter at the airgap

D_{ri} = Shaft diameter

h_m = PM thickness

PPM = PM Span

γ_{cu} = Specific weight of the iron

$kmag\_t$ = Teeth iron losses safety coefficient

$kmag\_bi$ = Back iron losses safety coefficient

k_{cart} = Carter coefficient

τ_p = Pole pitch

τ_u = Slot pitch

A = Electrical loading

B = Magnetic loading

Acronyms

PMSR = Permanent Magnet Synchronous Generator

SynR = Synchronous Reluctance

FEM = Finite Element Analysis

MTPA = Maximum Torque Per Ampere

PMs = Permanent Magnet

SMPM = Surface Mount Permanet Motor

PMASR = Magnet Assisted Synchronous Reluctance

NdFeB = Neodymium

SEG REL = Segmented Reluctance

PWM = Pulse Width Modulation

IPM = Interior Permanet Magnet